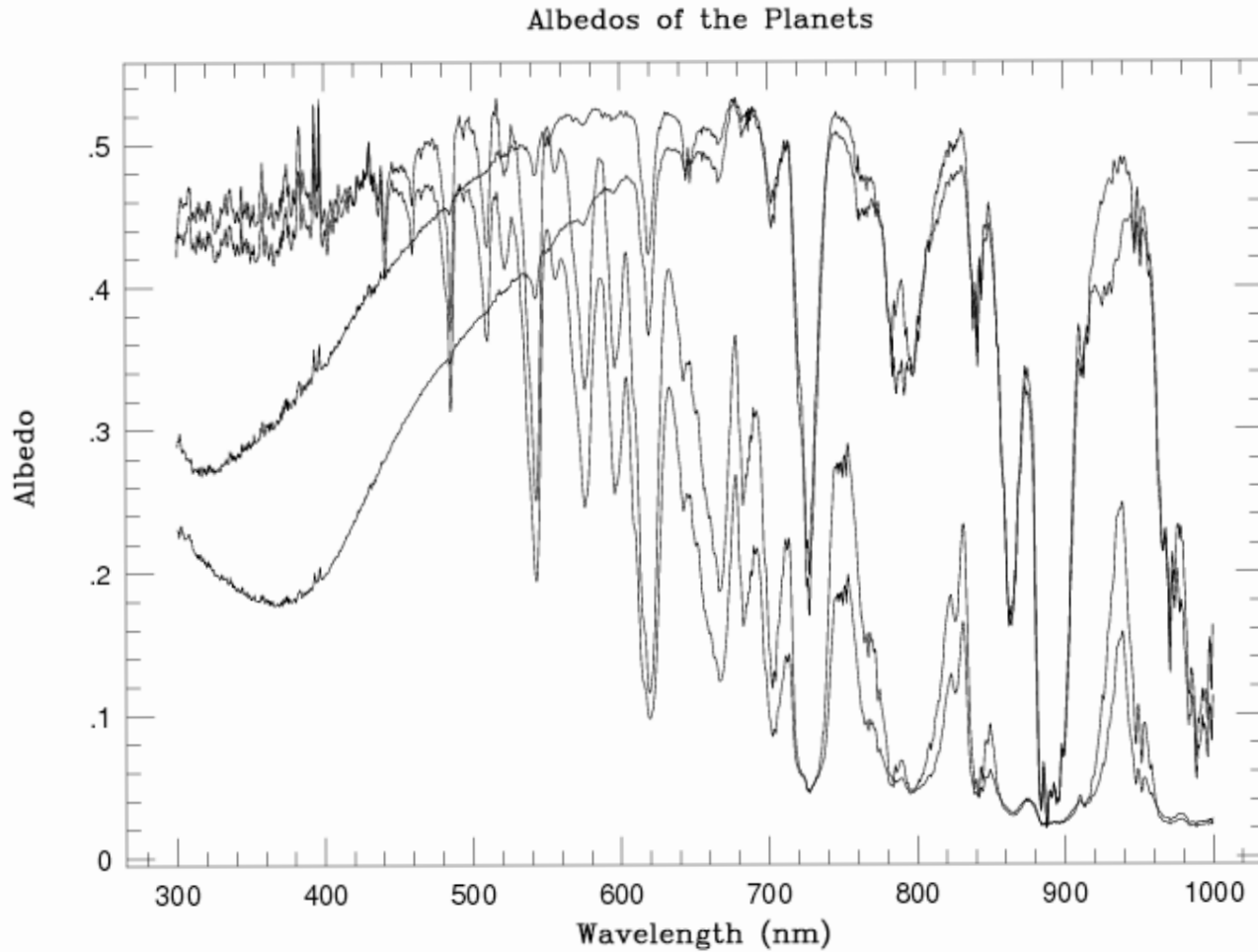
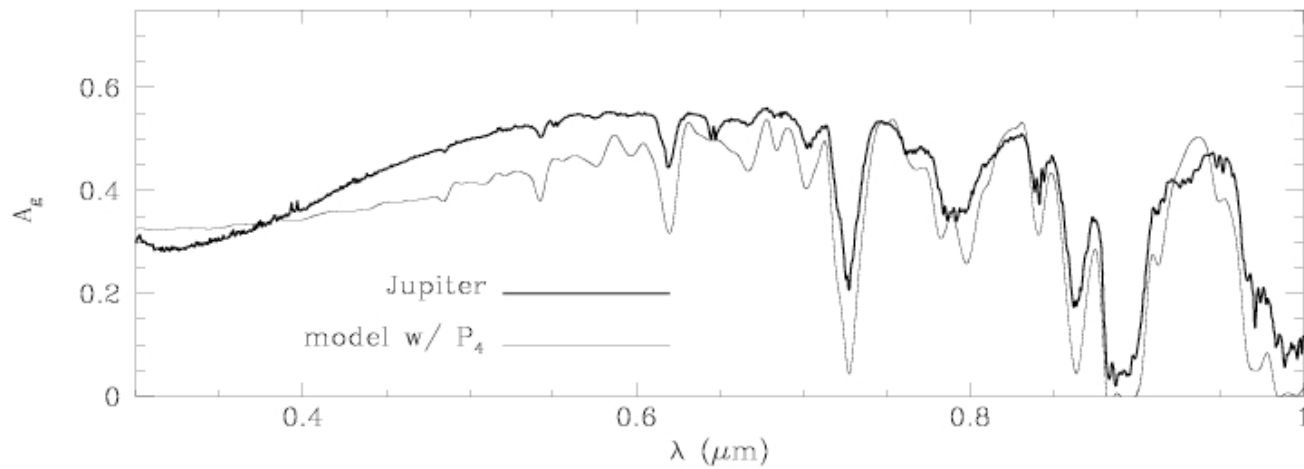
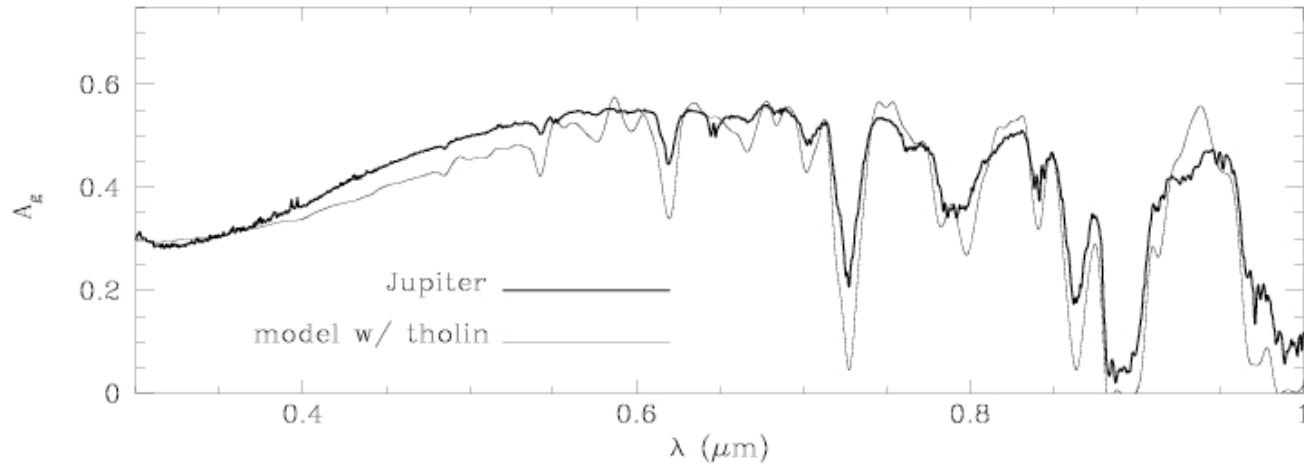


The **Planet/Star Flux Ratio** for wide-separation extra-solar giant planets (EGPs) depends upon:

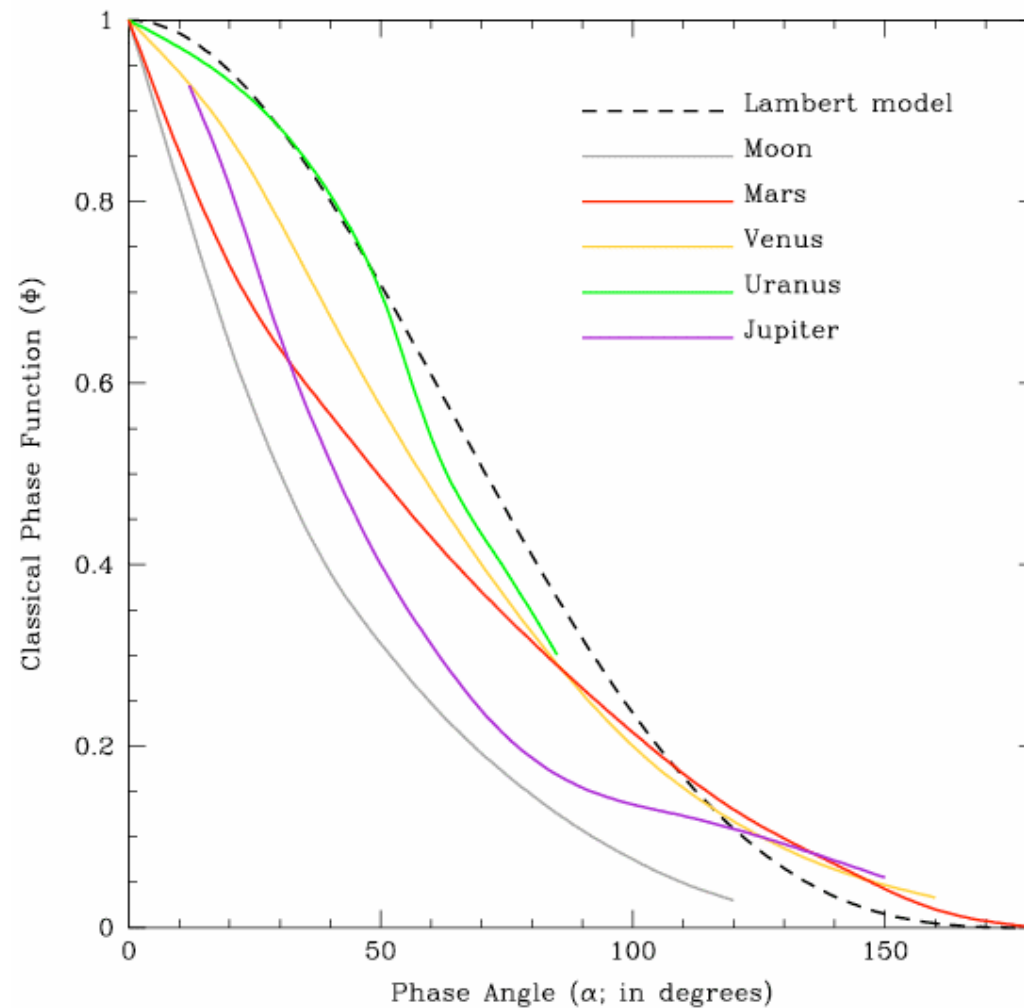
- **Geometric albedo** (A_g), **Phase Function** ($\Phi(\alpha)$), **Keplerian elements**, Epoch
- Both A_g and $\Phi(\alpha)$ **depend upon wavelength** (!) - planet color a function of phase
- Temperature-pressure-composition profiles are needed
- **Clouds** (NH_3 and H_2O) are crucial determinants, as are **Hazes** (polyacetylenes, tholins, ...)
- For clouds and hazes: Need particle-size distributions, complex indices, vertical extent
- **Polarization** can be a useful adjunct for physical interpretation
- Detailed models, simple models, and analytic approximations are available, but **work is needed to develop analysis pipeline** and reverse modeling protocols to extract physical parameters, with error bars.



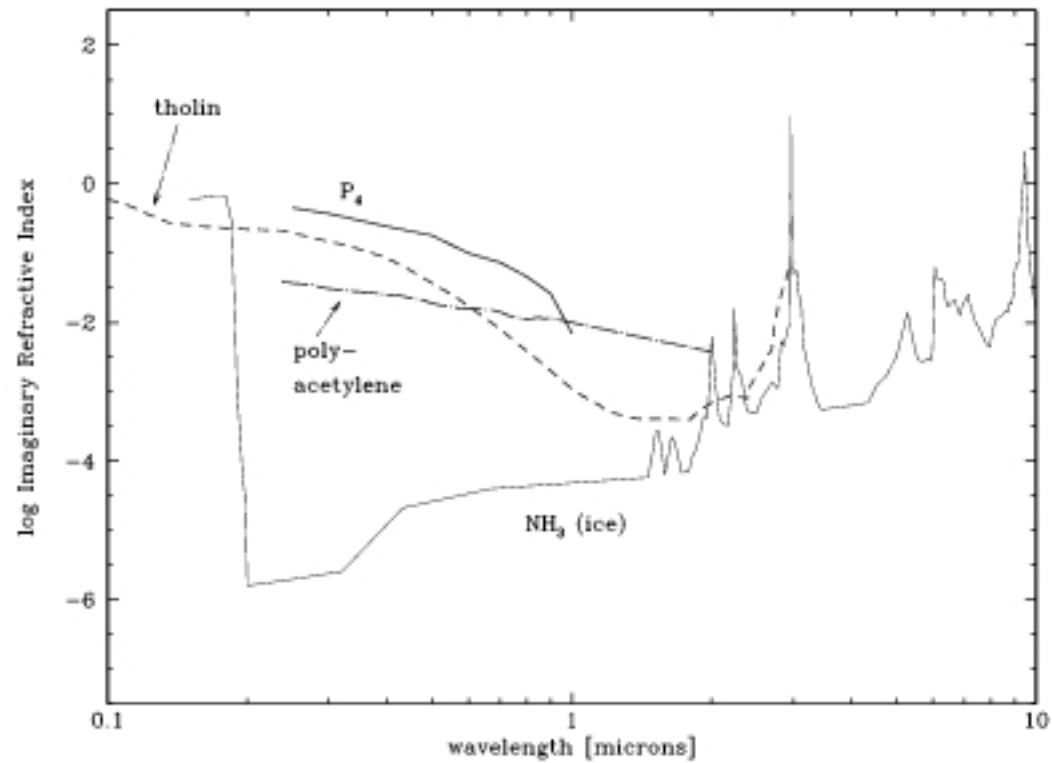
Geometric albedos of Jupiter, Saturn, Uranus, and Neptune in the optical (from Karkoscha 1994).



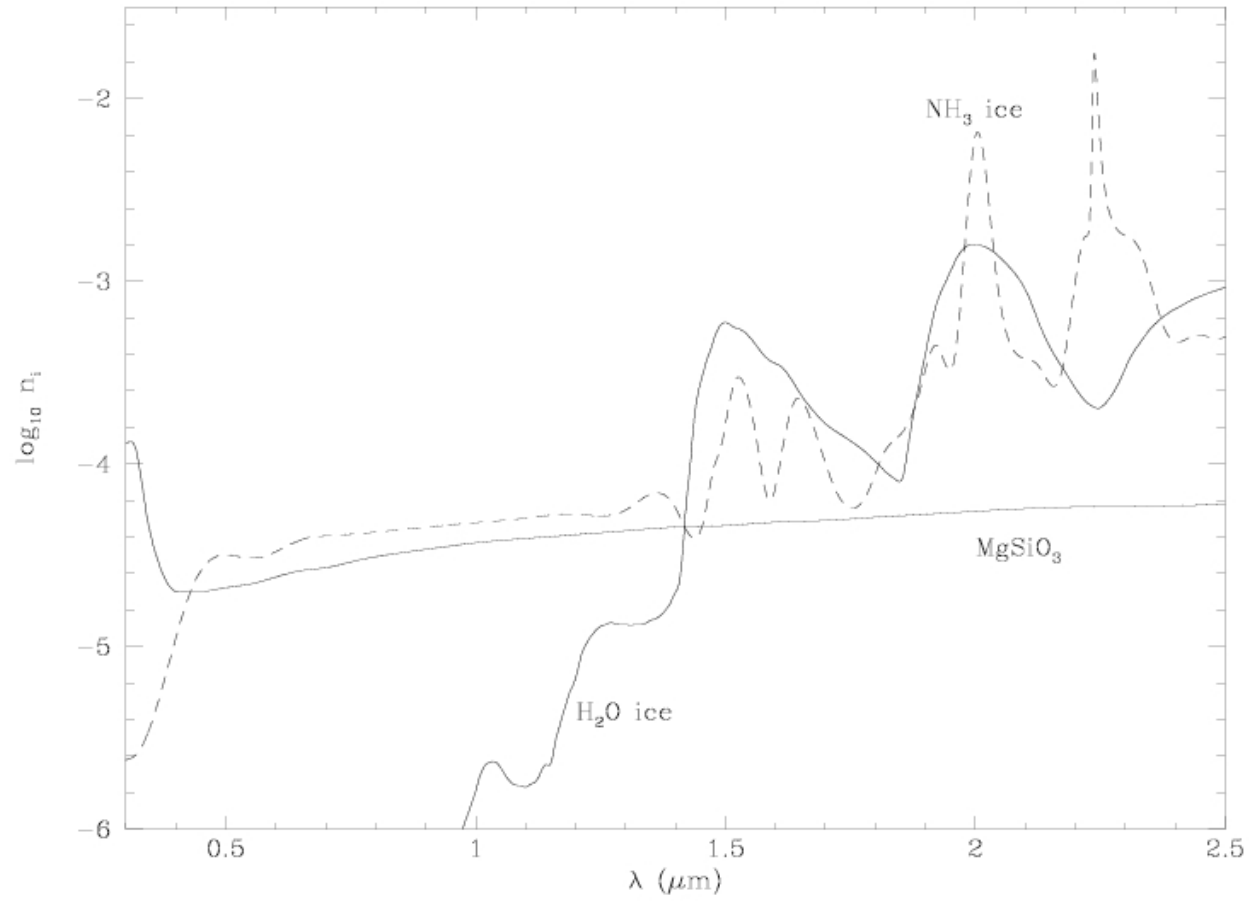
The geometric albedo spectrum of Jupiter compared with models (thin curves). The top model utilizes tholin as a chromophore, while the bottom model uses P_4 .



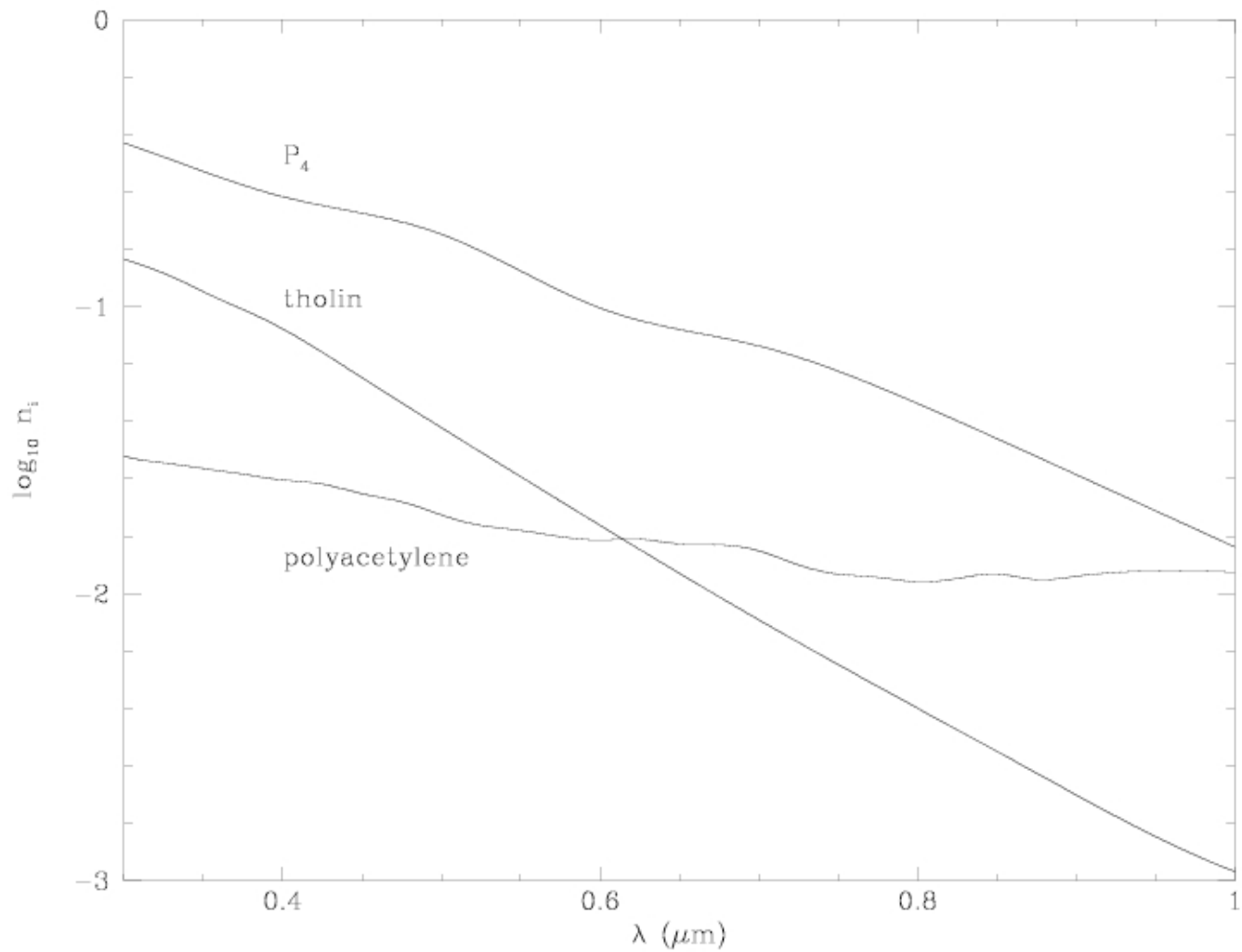
The measured visual phase functions for a selection of Solar System objects. A Lambert scattering phase curve, for which radiation is scattered isotropically off the surface regardless of its angle of incidence, is shown for comparison. The phase functions of the Moon and Mars peak near full phase (the so-called "opposition effect"). A red bandpass Jupiter phase function, taken from Dyudina et al. (2004), is also plotted.



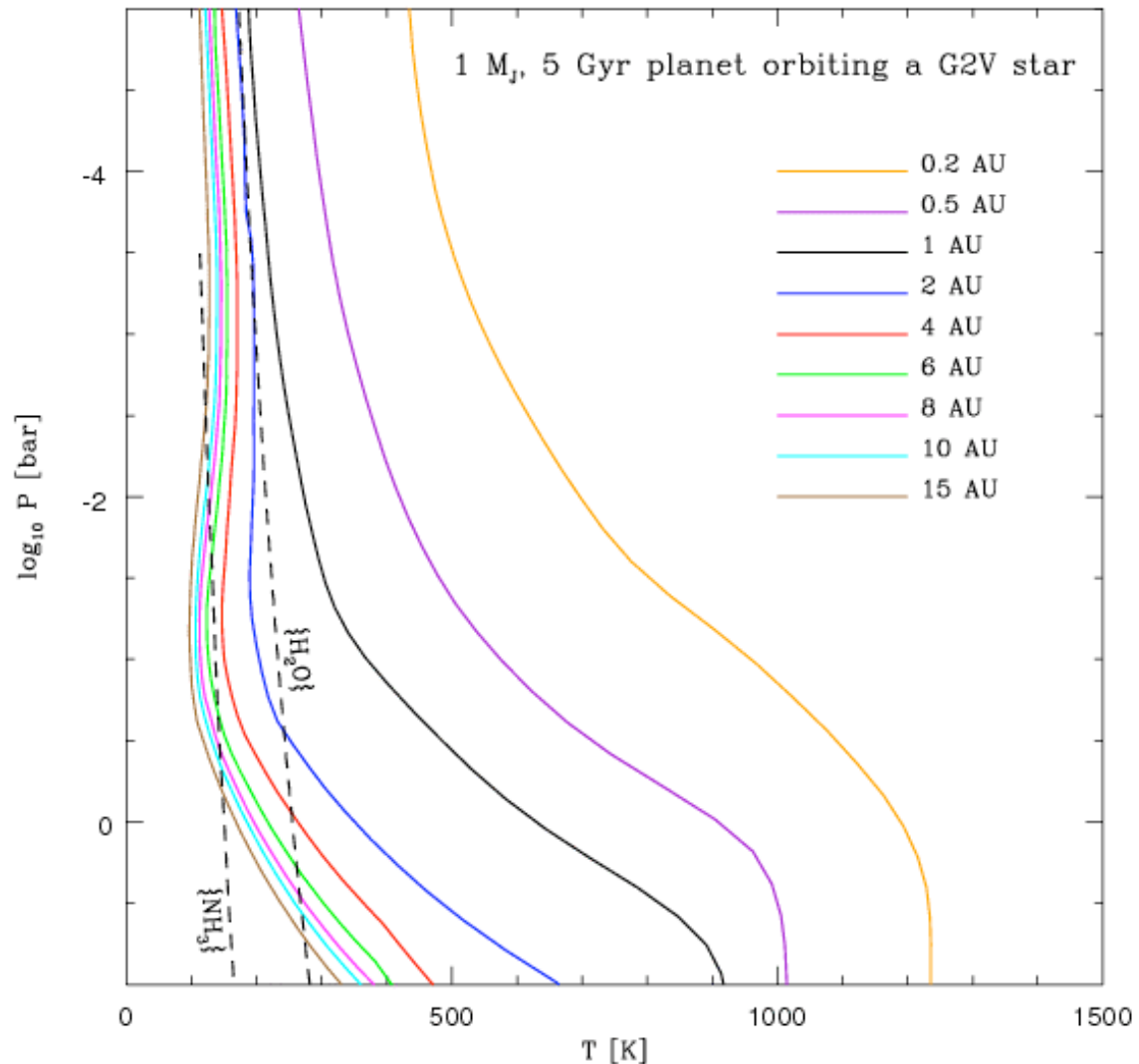
Imaginary indices of refraction for possible haze chromophores, in comparison to that for NH₃ (ice).



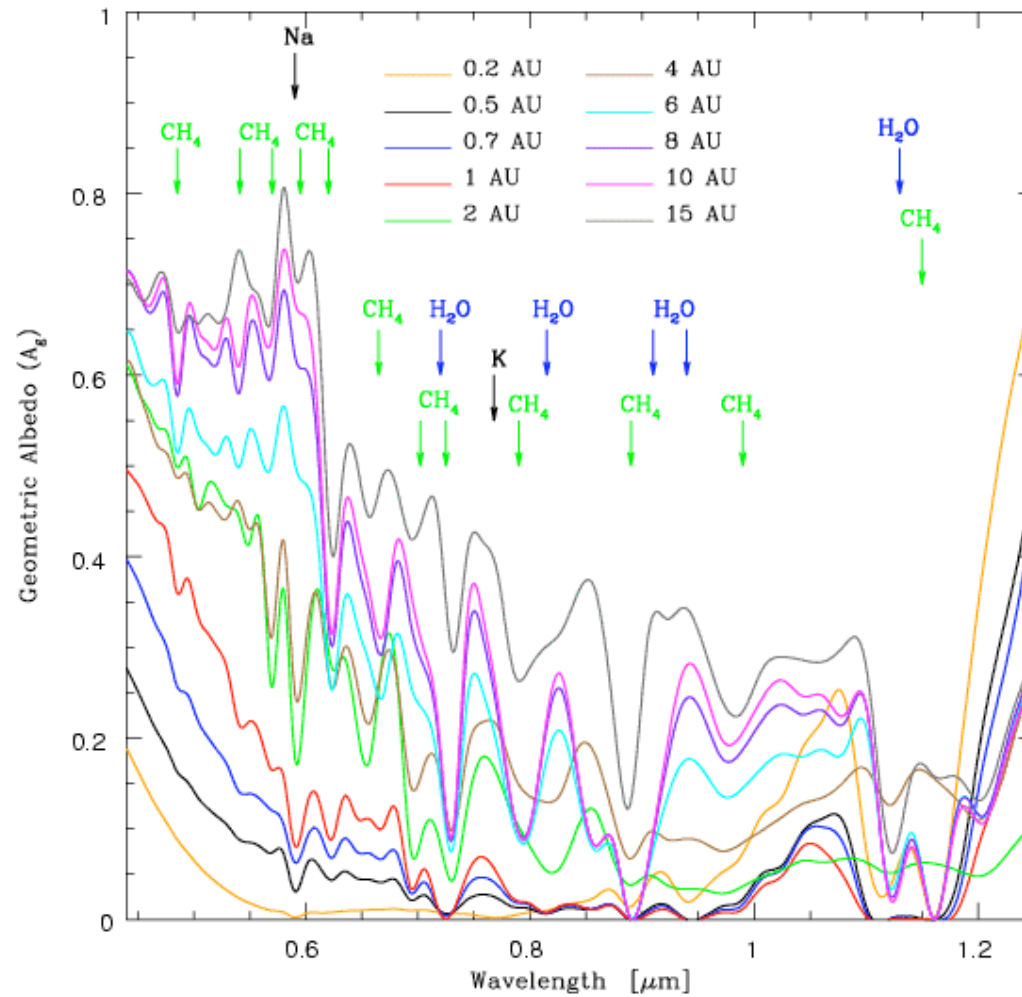
Imaginary refractive indices of the principal condensates.



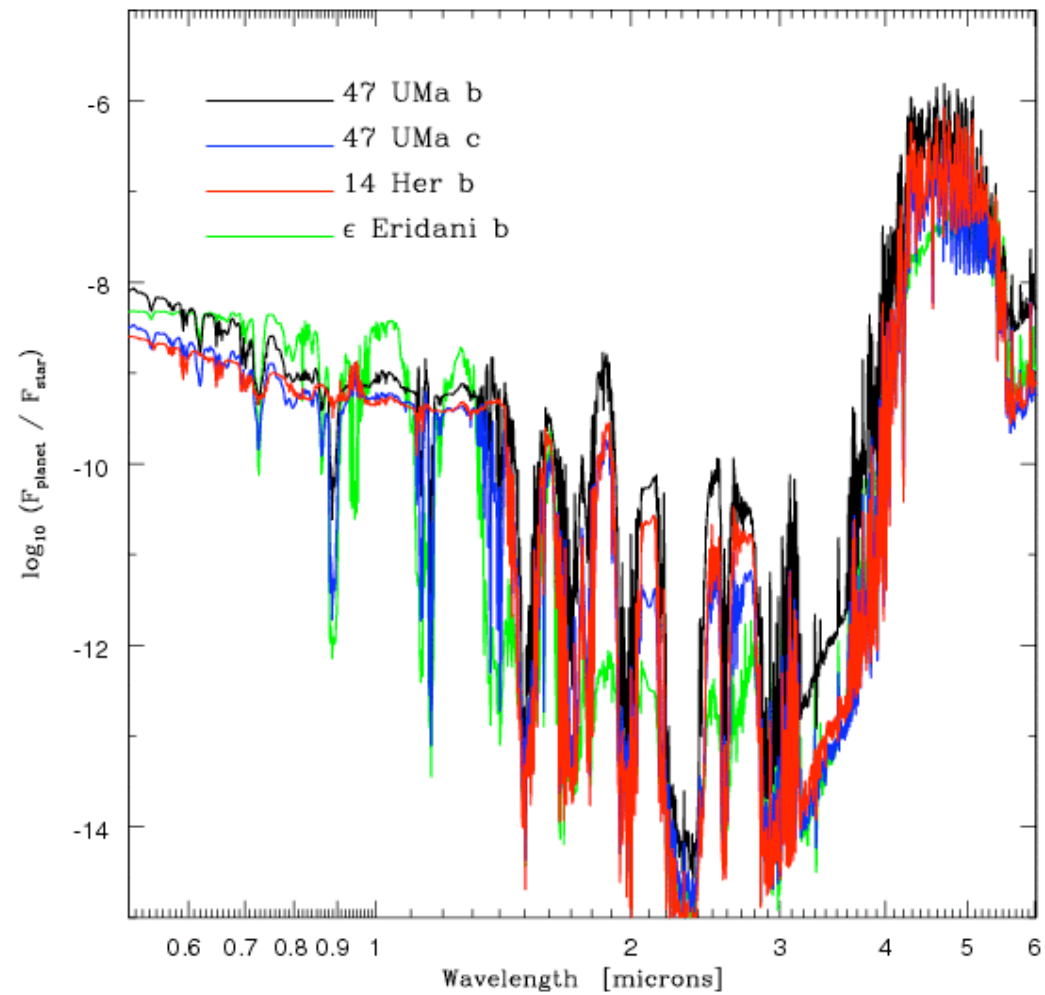
Imaginary refractive indices of stratospheric haze and tropospheric chromophore candidates. Tholin and P_4 provide a great deal of absorption in the UV/blue.



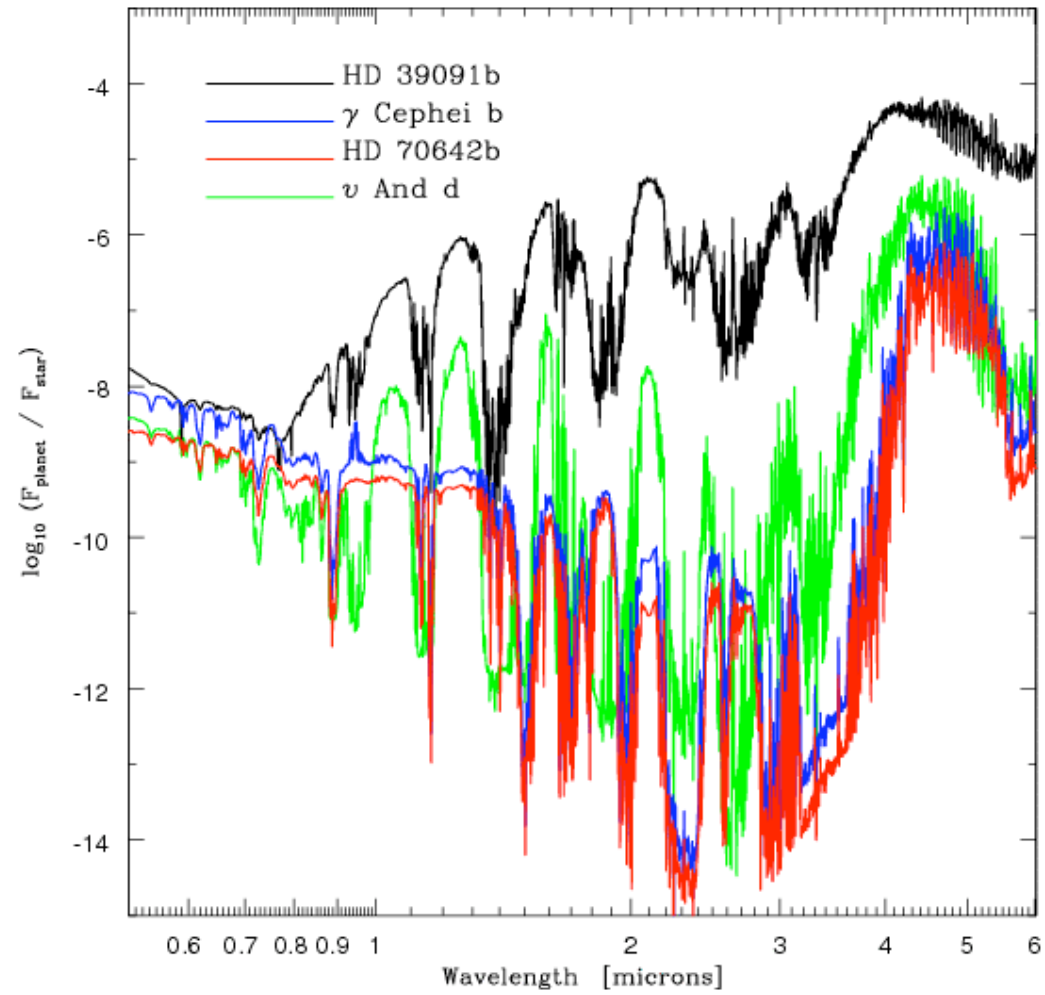
The temperature-pressure (T-P) profiles for a selection of model EGPs. Condensation curves for water and ammonia are shown. The deeper intersections of these condensation curves with the T-P profiles indicate the positions of the cloud bases.



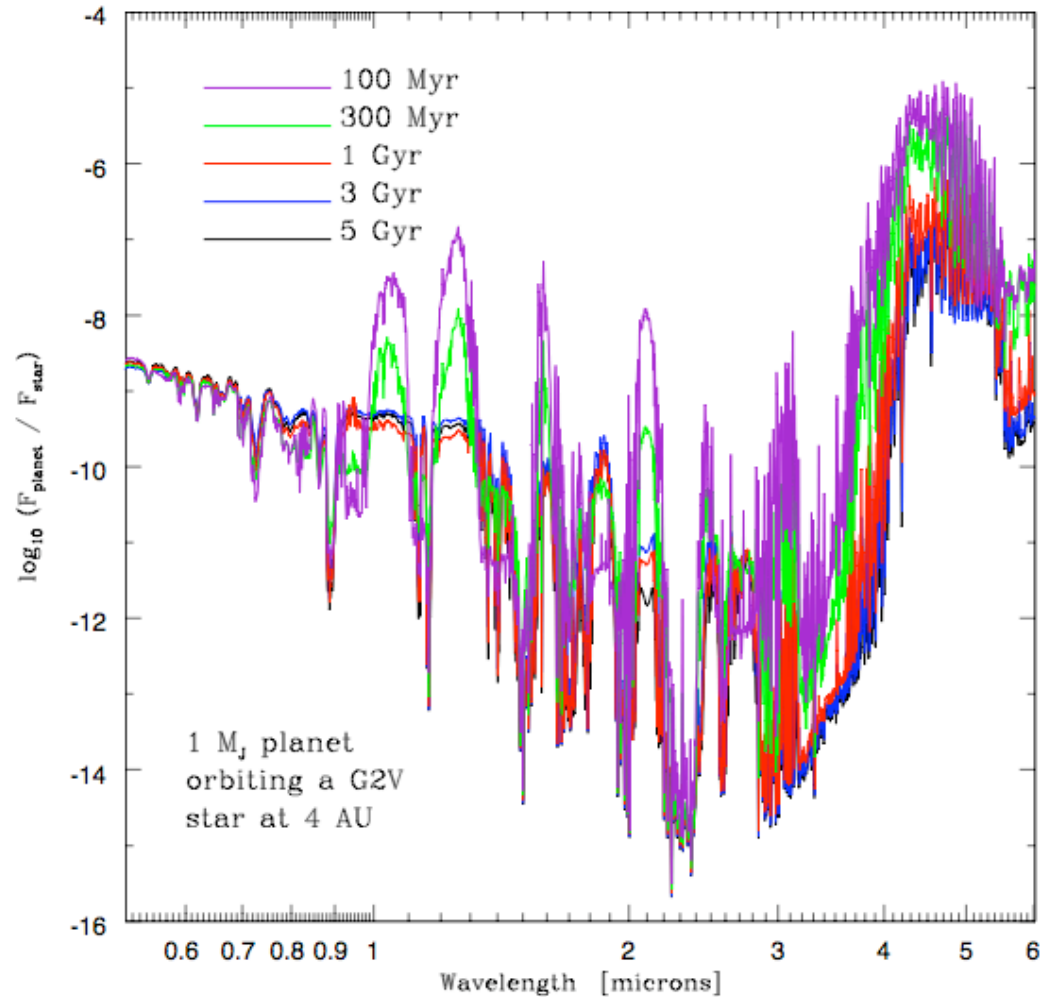
Low-resolution, wavelength-dependent geometric albedos of 1-M_J, 5 Gyr EGPs ranging in orbital distance from 0.2 AU to 15 AU about a G2V star. Cubic splines are fit to all albedo data. Reddening effects of photochemical hazes are not incorporated.



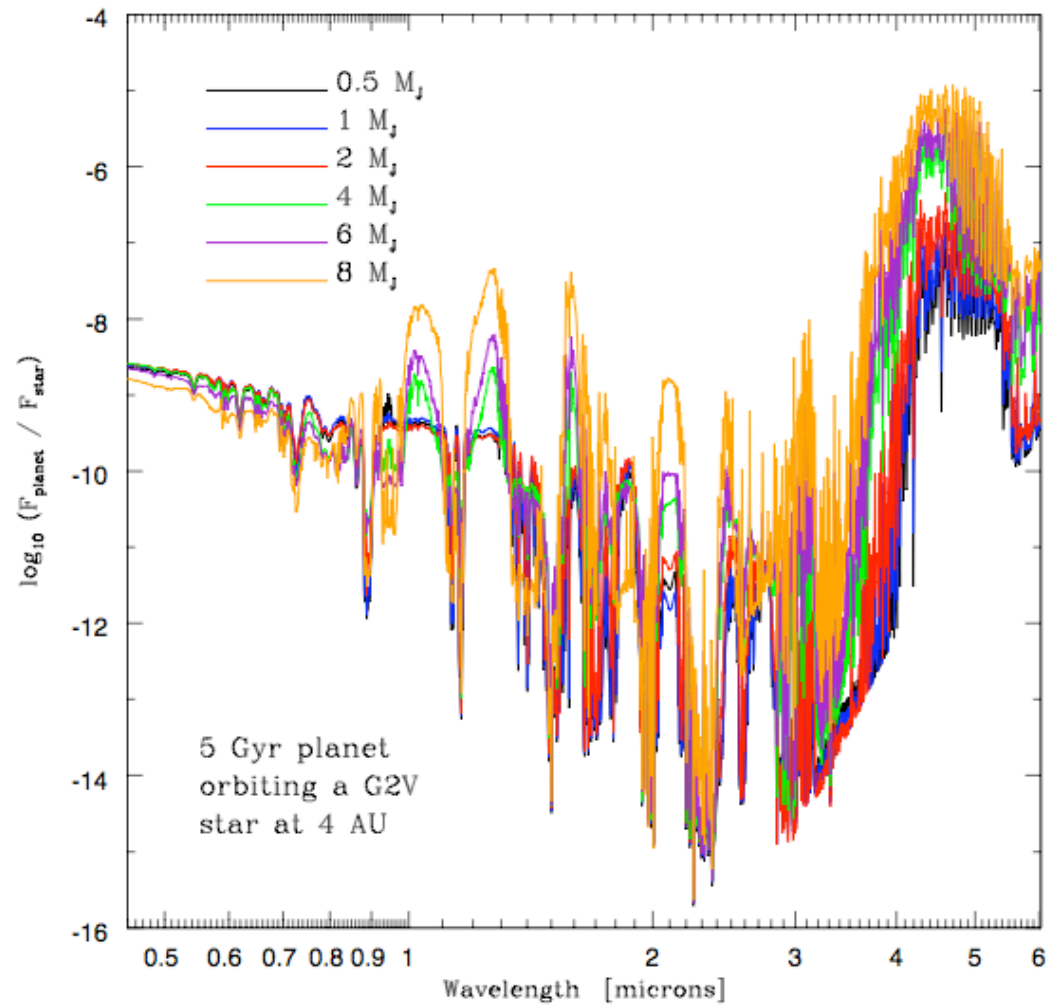
Average Planet/Star flux ratios for some representative non-transiting EGPs.



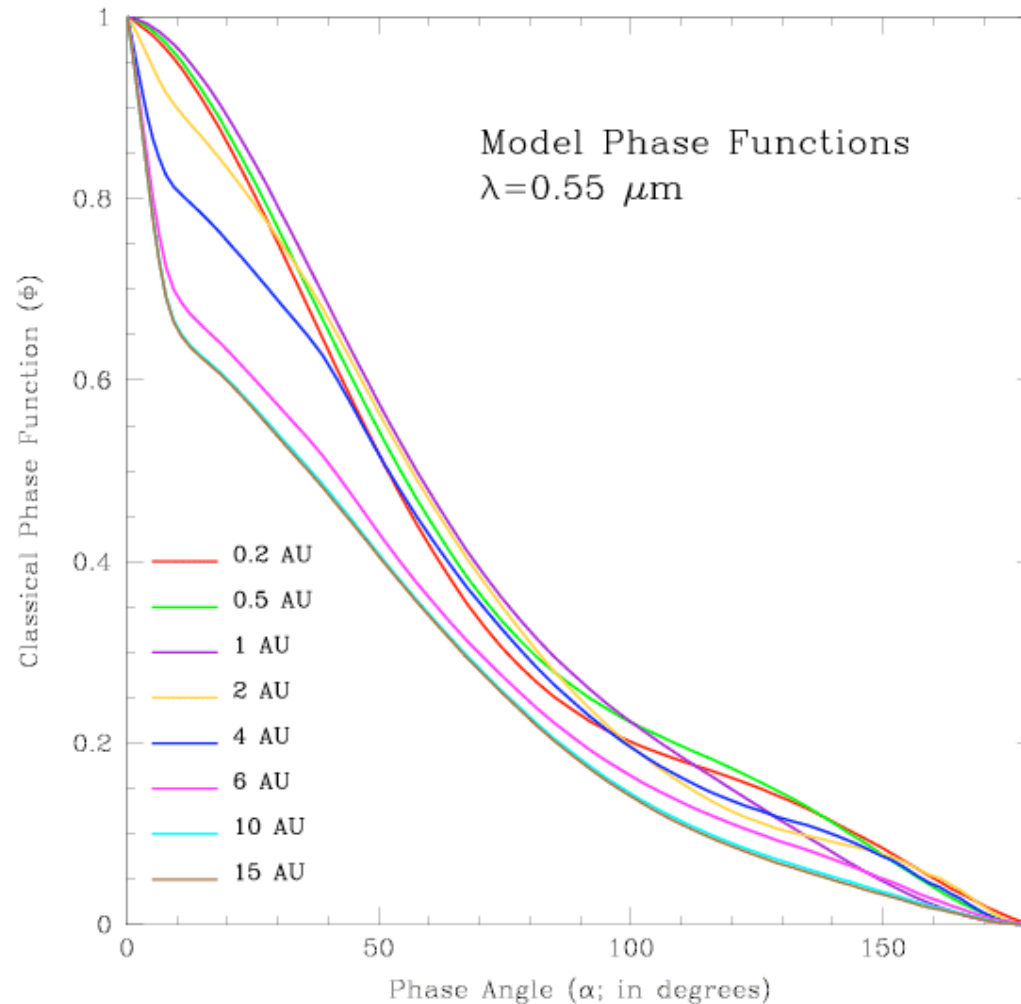
Average Planet/Star flux ratios for some other representative non-transiting EGPs.



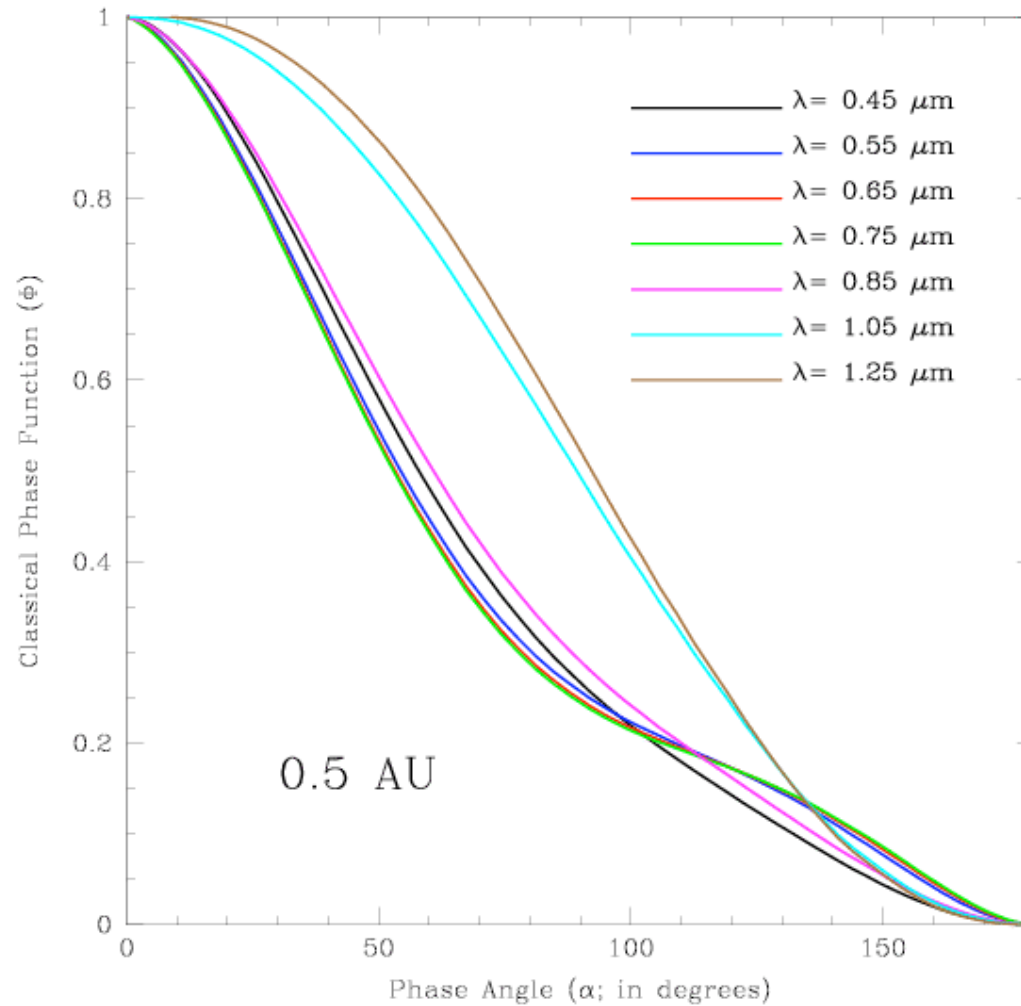
Planet/Star flux ratios as a function of age for a given EGP mass (1 M_J) orbiting a G2V star at 4 AU.



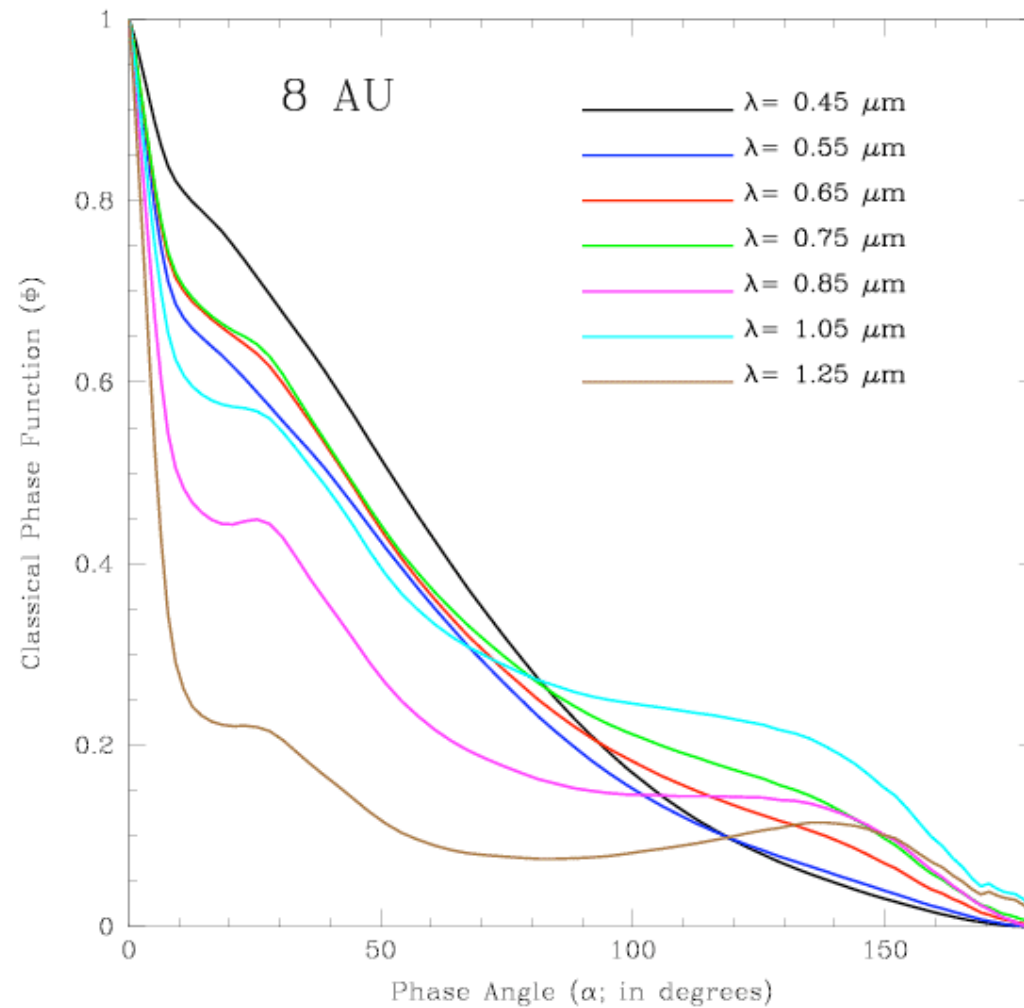
Planet/Star flux ratios as a function EGP mass at an age of 5 Gyrs, orbiting a G2V star at 4 AU.



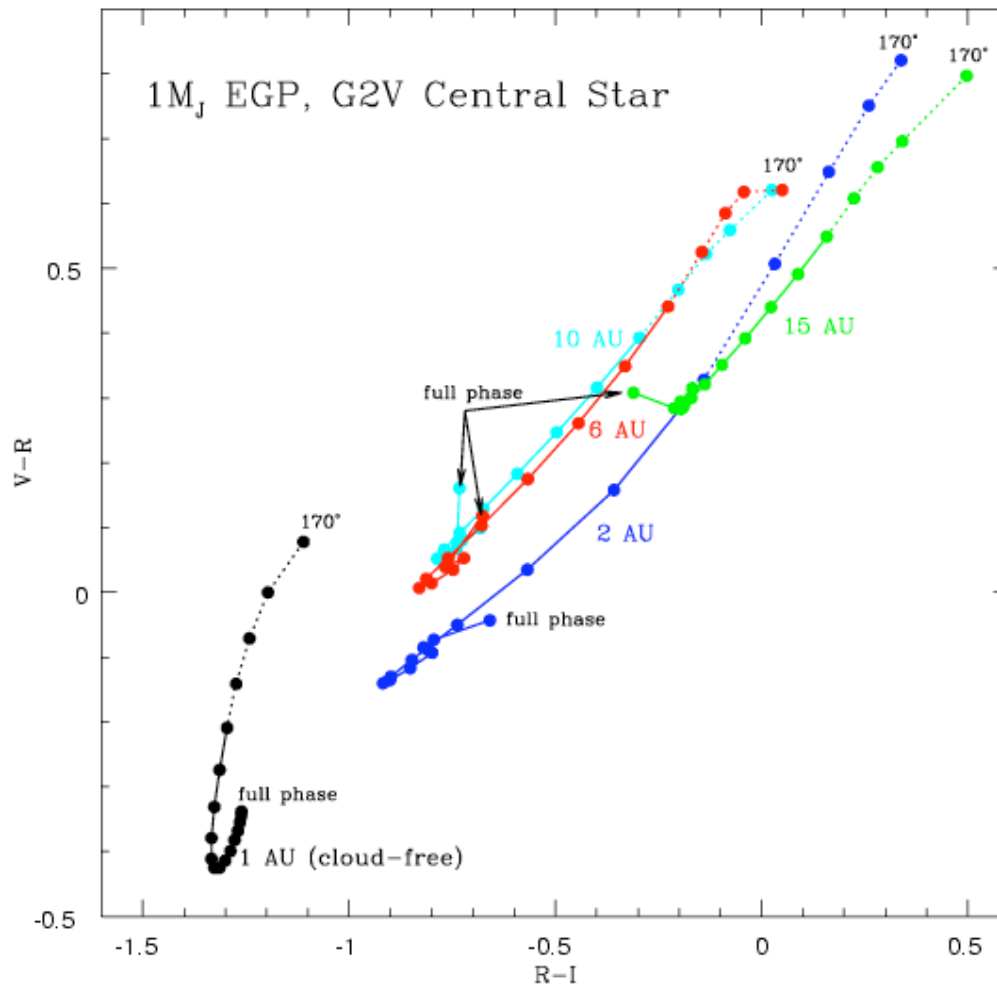
Theoretical optical phase functions of 1- M_J , 5-Gyr EGPs ranging in orbital distance from 0.2 AU to 15 AU from a G2V star. Near full phase, the phase functions for our baseline models at larger orbital distances peak most strongly. For the cloud-free EGPs at smaller orbital distances (0.2 AU, 0.5 AU, and 1 AU), the phase functions are more rounded near full phase.



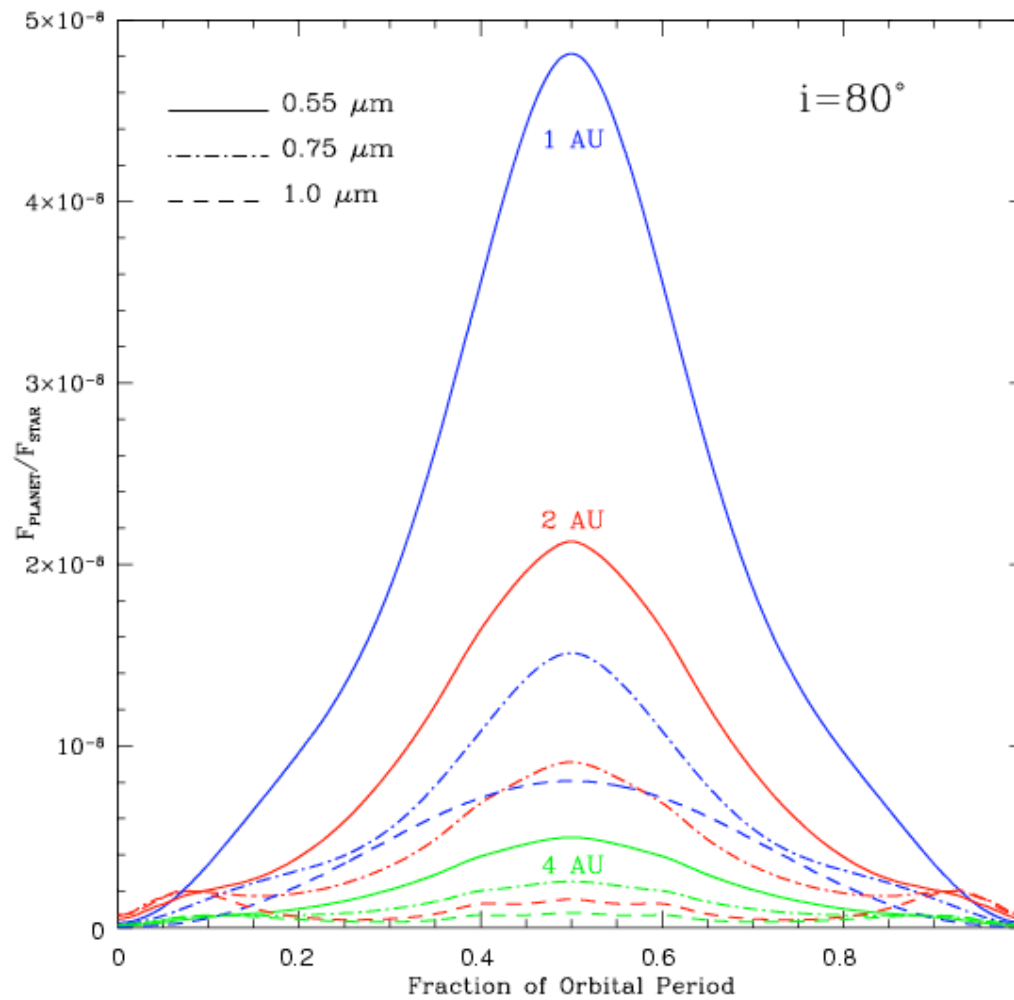
Wavelength dependence of the phase function for a cloud-free EGP orbiting at a distance of 0.5 AU from its G2V central star. The 1.05 microns and 1.25 microns phase curves are outliers because they contain a mix of thermally re-emitted and reflected radiation.



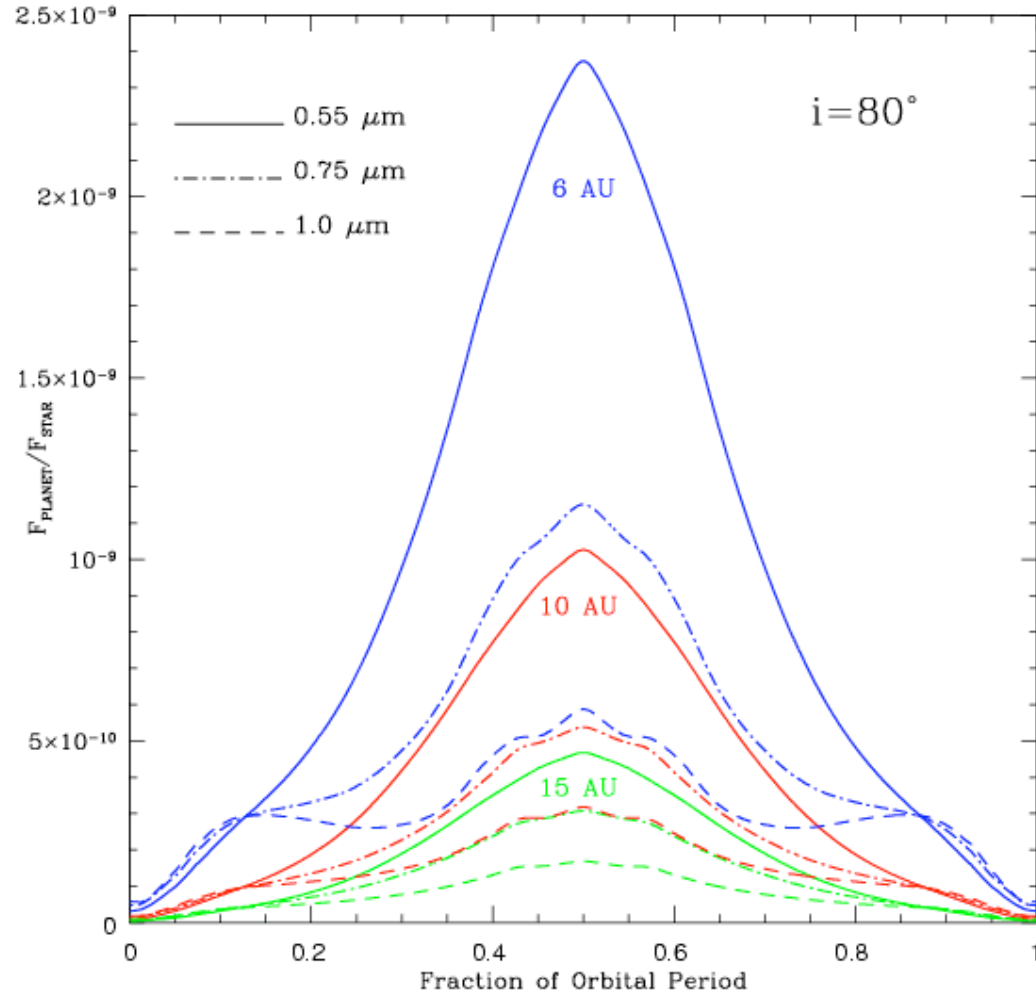
Wavelength dependence of the phase function for an EGP orbiting at a distance of 8 AU from its G2V central star. The EGP contains an ammonia cloud layer above a deeper water cloud.



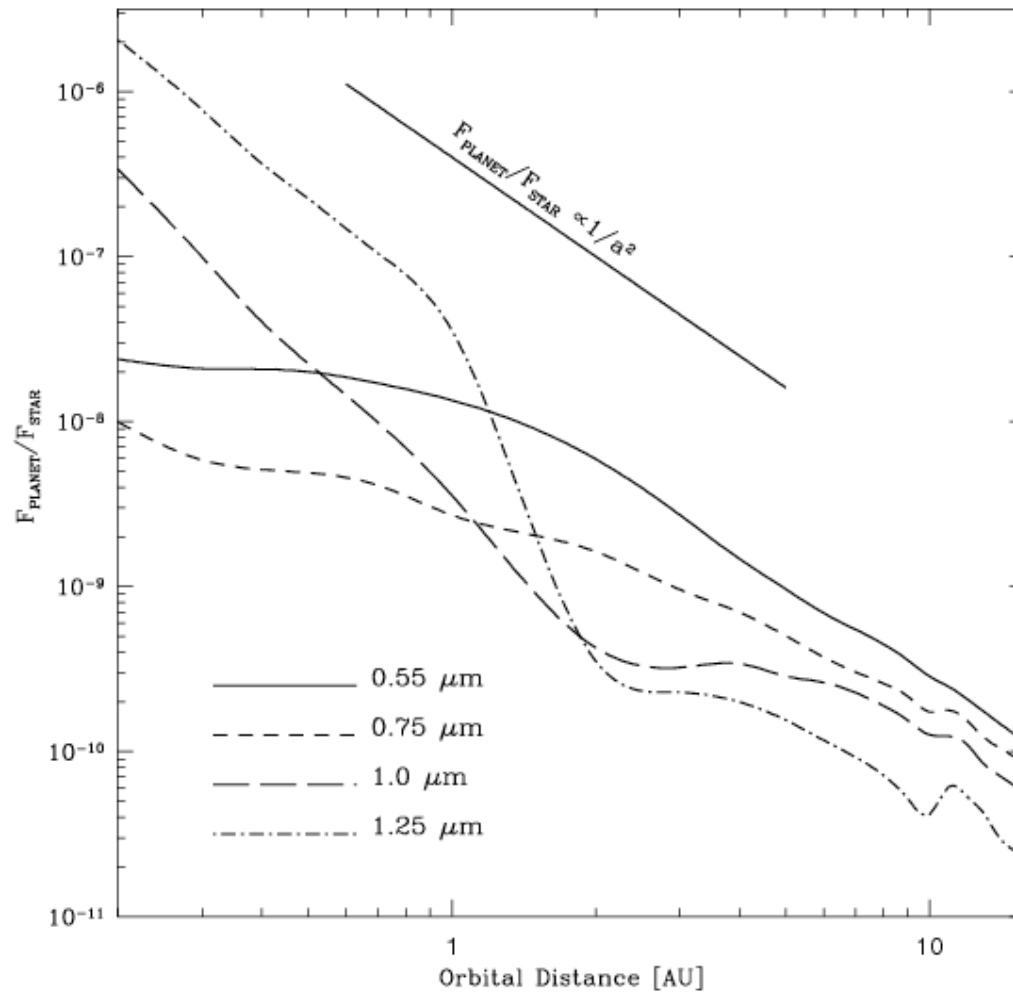
V-R vs. R-I color-color diagram detailing variations with planetary phase for a variety of orbital distances. Each of the curves depicts an orbit from full phase (0 degrees) to a thin crescent phase (170 degrees) in increments of 10 degrees (as indicated by the filled circles). Cloud-free EGPs are bluest near greatest elongation, while cloudy EGPs tend to be bluest in a gibbous phase. As full phase is approached, the colors redden somewhat. However, the crescent phases appear to be far redder, varying by as much as a full astronomical magnitude from their blue gibbous-phase colors in some cases. See text for details and a discussion of the accuracy at large phase angles (denoted by dotted lines).



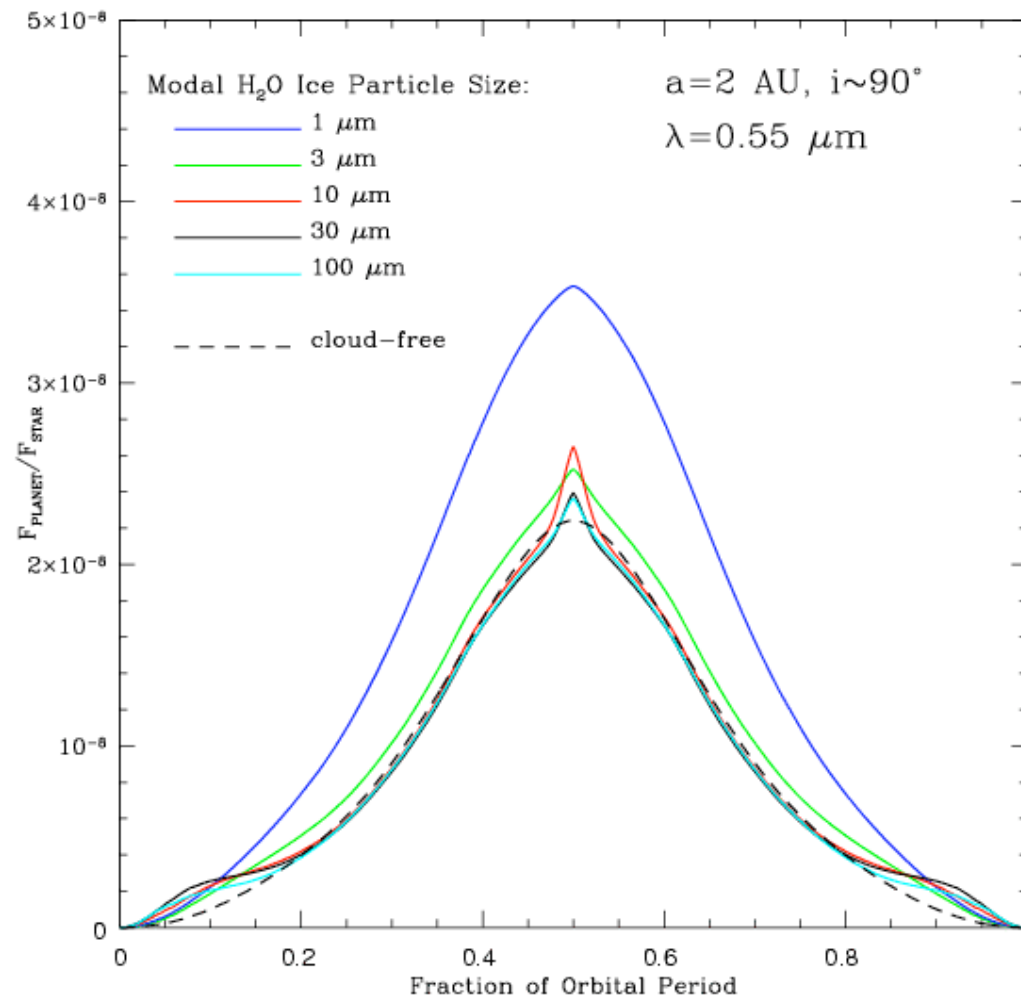
Light curves at 0.55, 0.75, and 1.0 microns for our model EGPs in circular orbits inclined to 80 degrees at distances of 1 AU, 2 AU, and 4 AU from a G2V star. The logarithm of the planet/star flux ratio is plotted. The models at 2 AU and 4 AU contain water ice clouds in their upper atmospheres, while the 1 AU model does not.



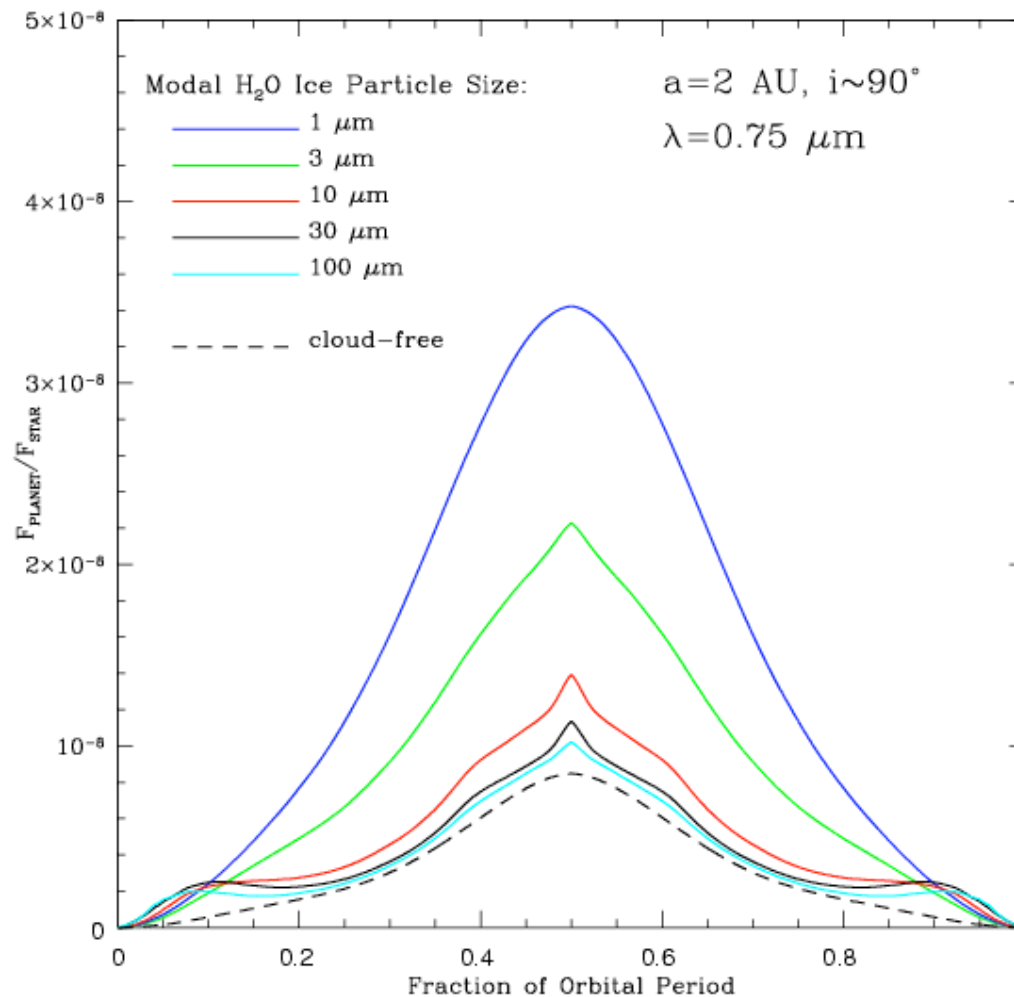
Light curves at 0.55, 0.75, and 1.0 microns for our model EGPs in circular orbits inclined to 80 degrees at distances of 6 AU, 10 AU, and 15 AU from a G2V star. The logarithm of the planet/star flux ratio is plotted. Each of these models contains an ammonia ice cloud layer above a deeper water cloud deck.



Planet/star flux ratio as a function of orbital distance at 0.55, 0.75, 1.0, and 1.25 microns assuming a G2V central star. In each case, the plotted value corresponds to a planet at greatest elongation with an orbital inclination of 80 degrees. Note that the planet/star flux ratios do not follow a simple $1/a^2$ law.

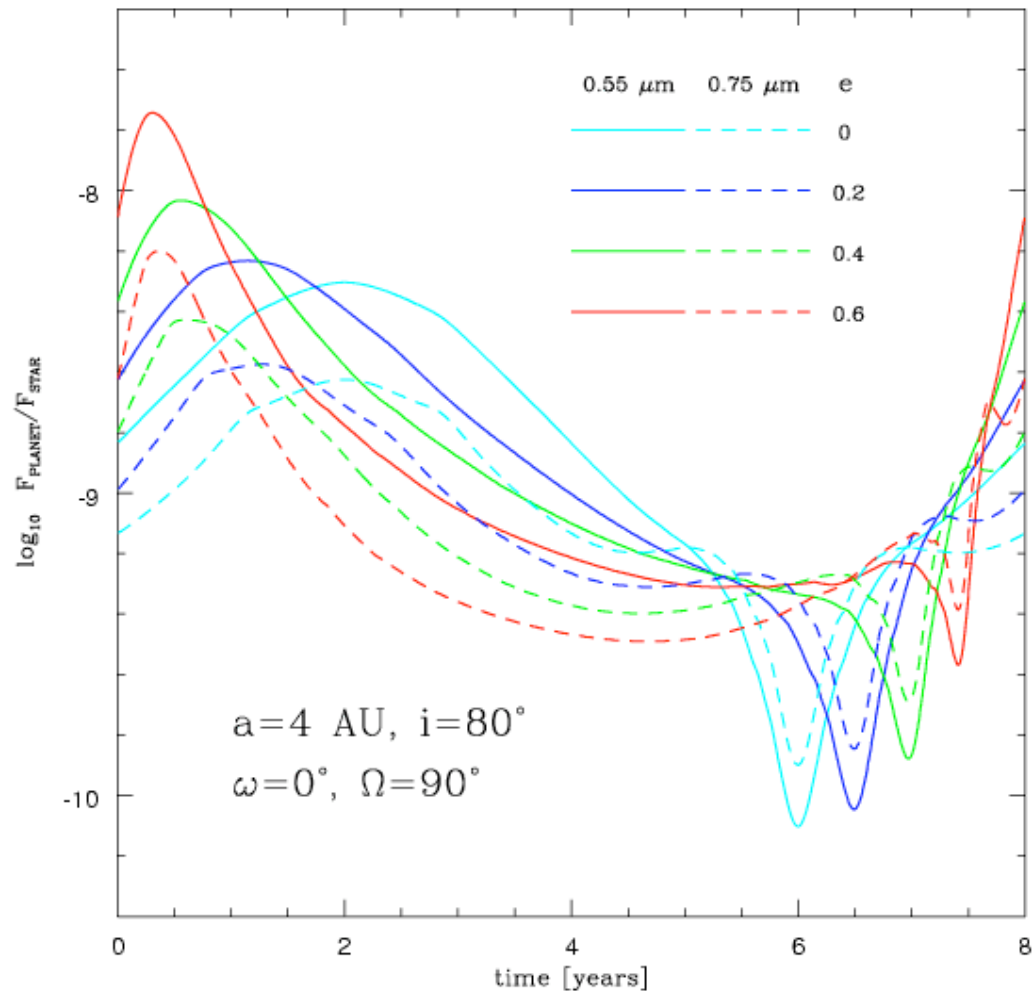


The dependence of the planet/star flux ratio on condensate particle size at a wavelength of 0.55 microns. Model light curves for EGPs at 2 AU with modal H₂O ice particle sizes of 1, 3, 10, 30, and 100 microns are depicted. Shown for comparison is a cloud-free model (black dashed curve). In order to show the full variation in the shapes and magnitudes of the light curves with particle size, we have set the orbital inclination to approximately 90 degrees so that the opposition effect, present for many of the models, can be seen in full.

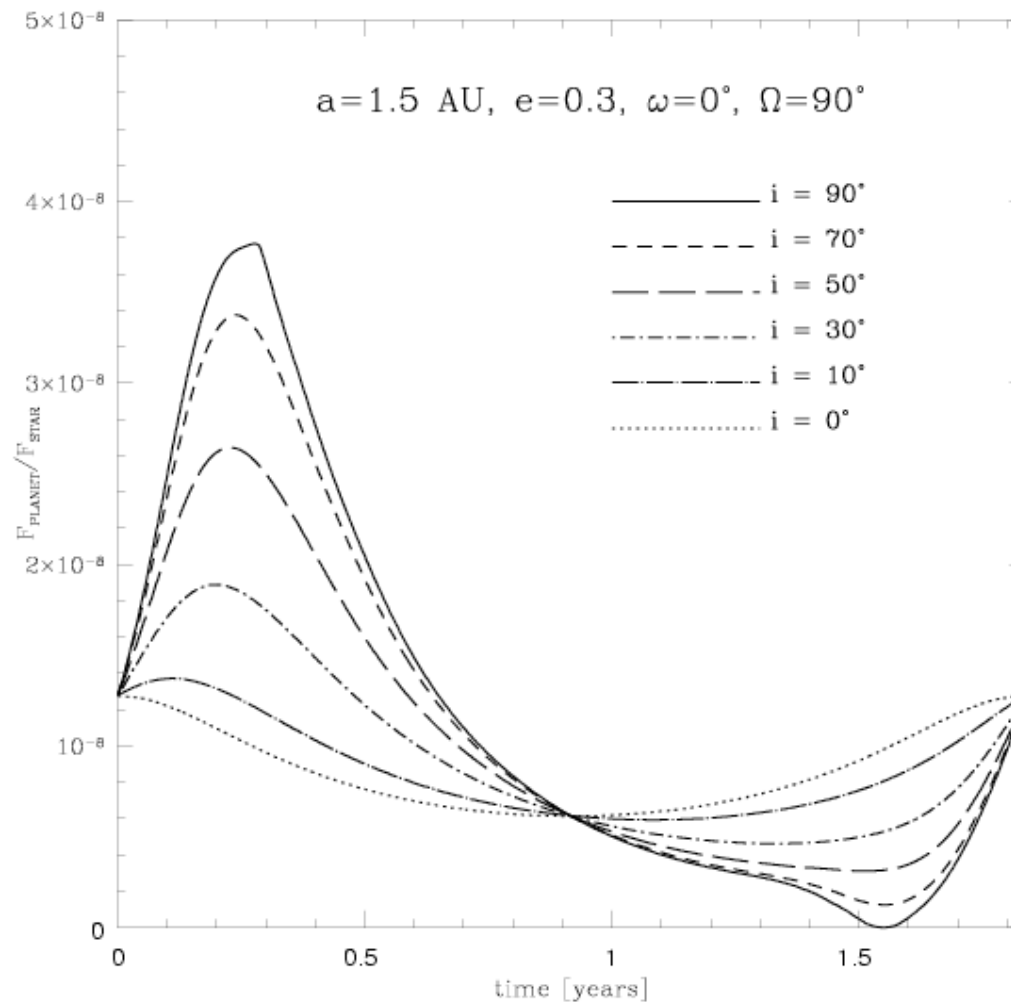


The dependence of the planet/star flux ratio on condensate particle size at a wavelength of 0.75 microns. Model light curves for EGPs at 2 AU with modal H₂O ice particle sizes of 1, 3, 10, 30, and 100 microns are depicted. Shown for comparison is a cloud-free model (black dashed curve).

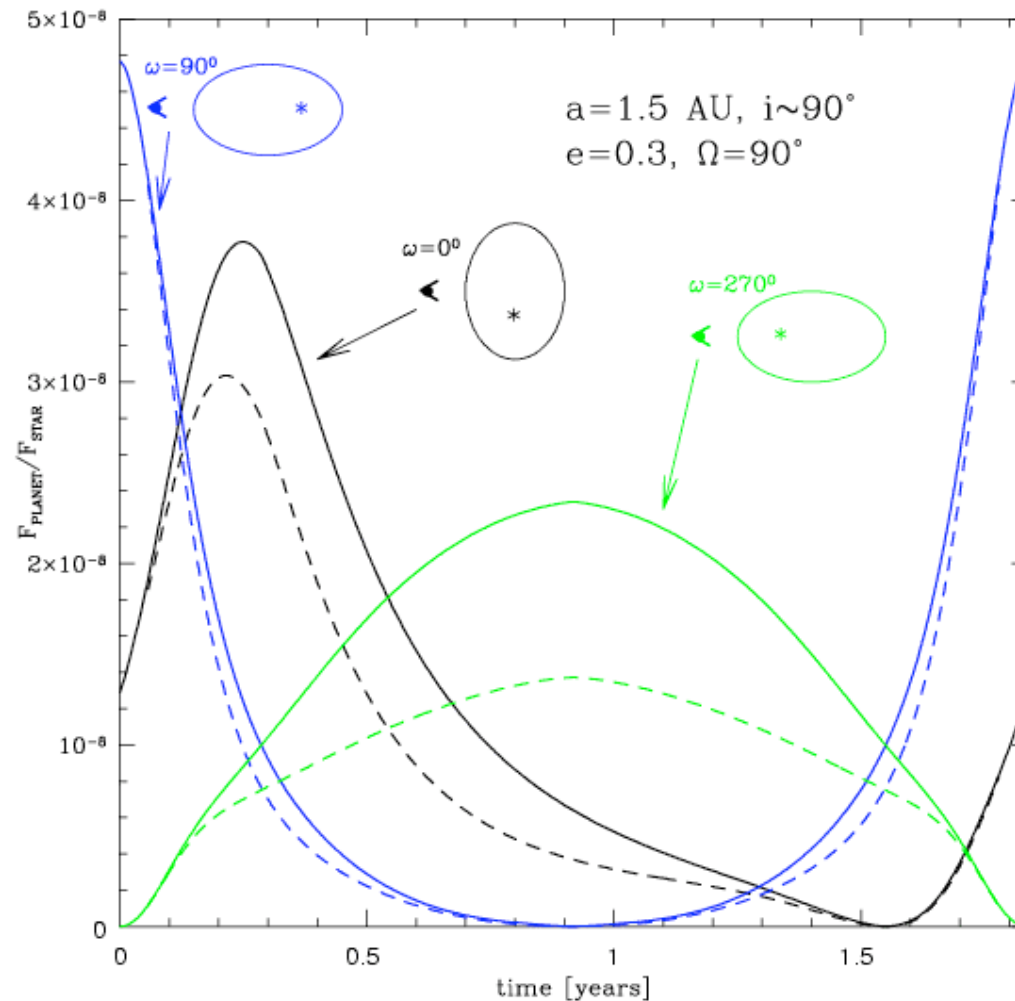
In order to show the full variation in the shapes and magnitudes of the light curves with particle size, we have set the orbital inclination to approximately 90 degrees so that the opposition effect, present for many of the models, can be seen in full.



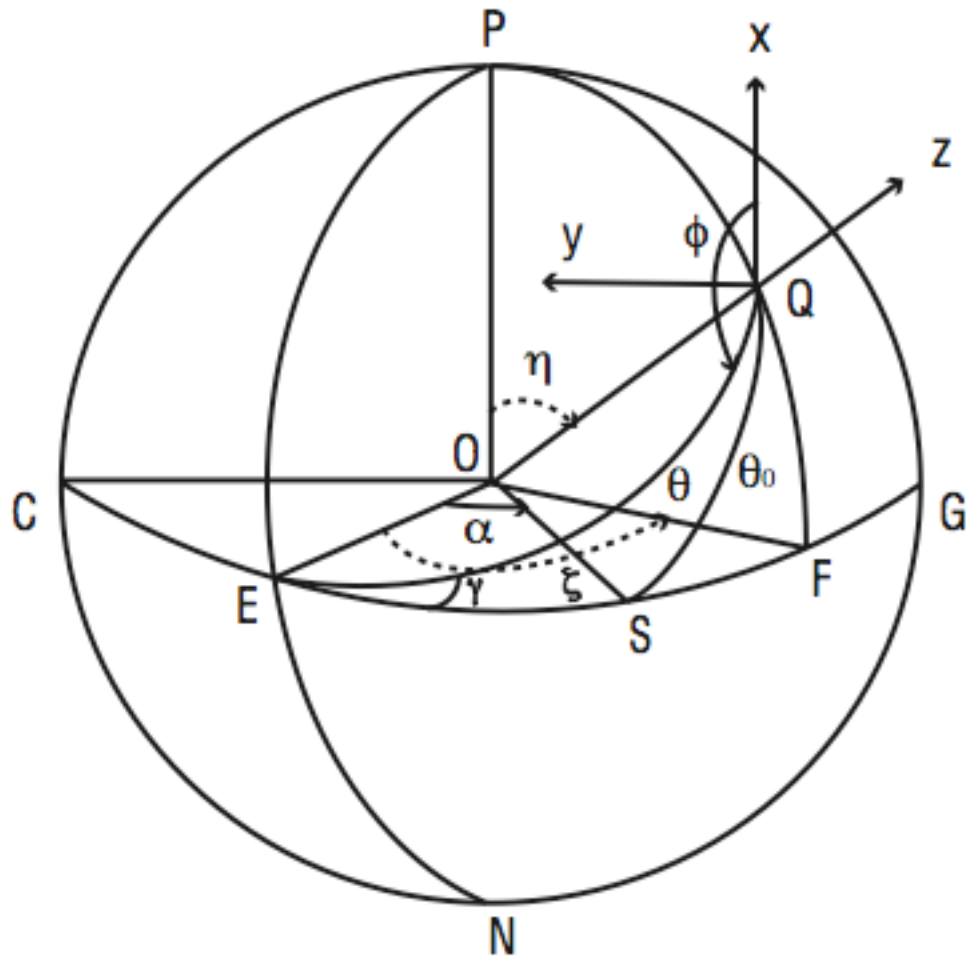
The logarithm of the optical (at 0.55 microns) and far red (0.75 microns) planet/star flux ratios as a function of eccentricity for $a = 4 \text{ AU}$, fixing i at 80 degrees and ω is zero. The planet/star flux ratio is a factor of 2 to 3 greater at 0.55 microns than in the far red at most planetary phases.



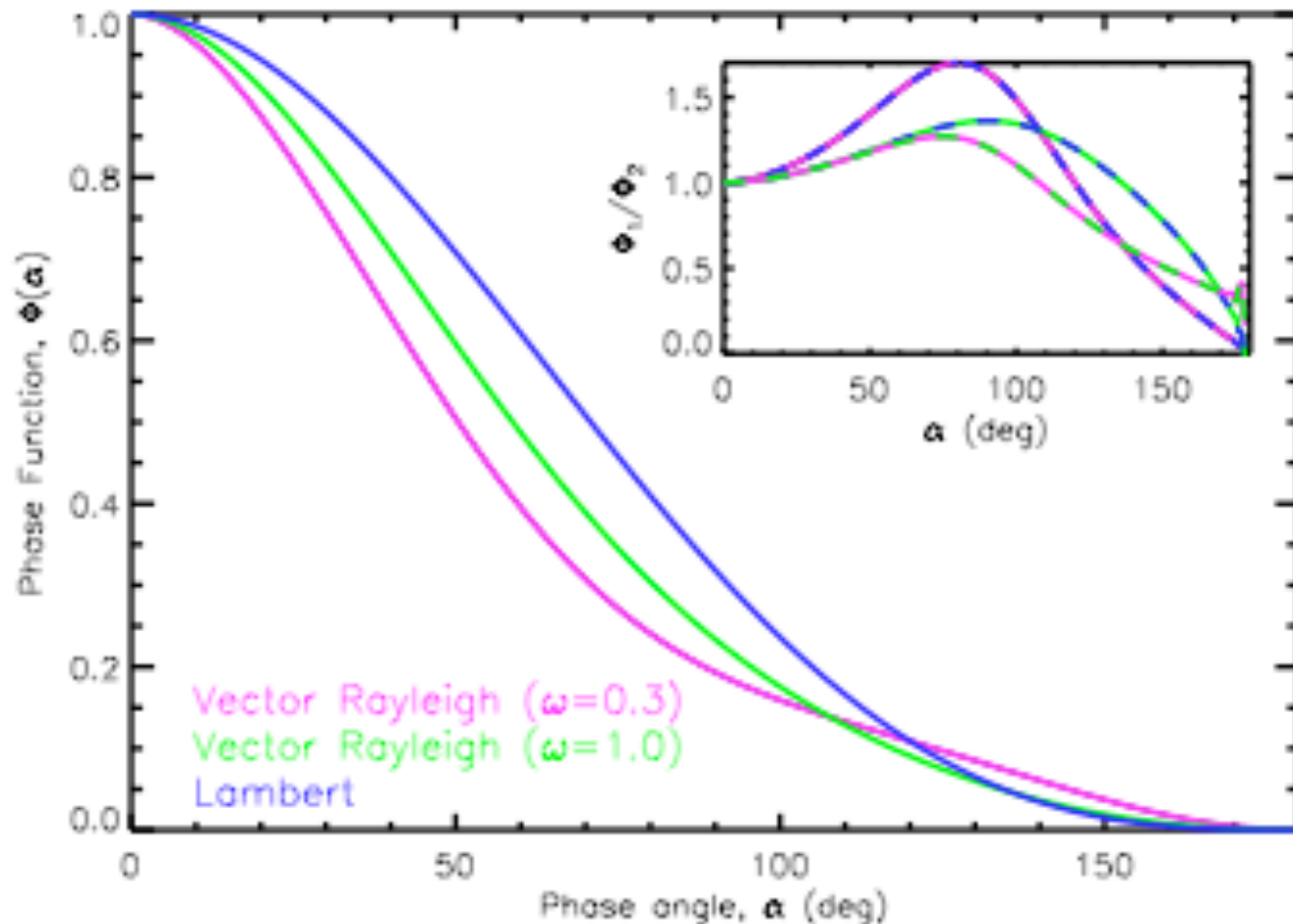
Variation with inclination of the optical light curve for an elliptical orbit (G2V central star, $a = 1.5 \text{ AU}$, $e = 0.3$). For a highly-inclined orbit, the peak of the planet/star flux ratio is a factor of ~ 3 greater than for a face-on ($i=0$ degrees) orbit. The (symmetric) variation for the face-on case is due entirely to the variation in the planet-star distance over an eccentric orbit.



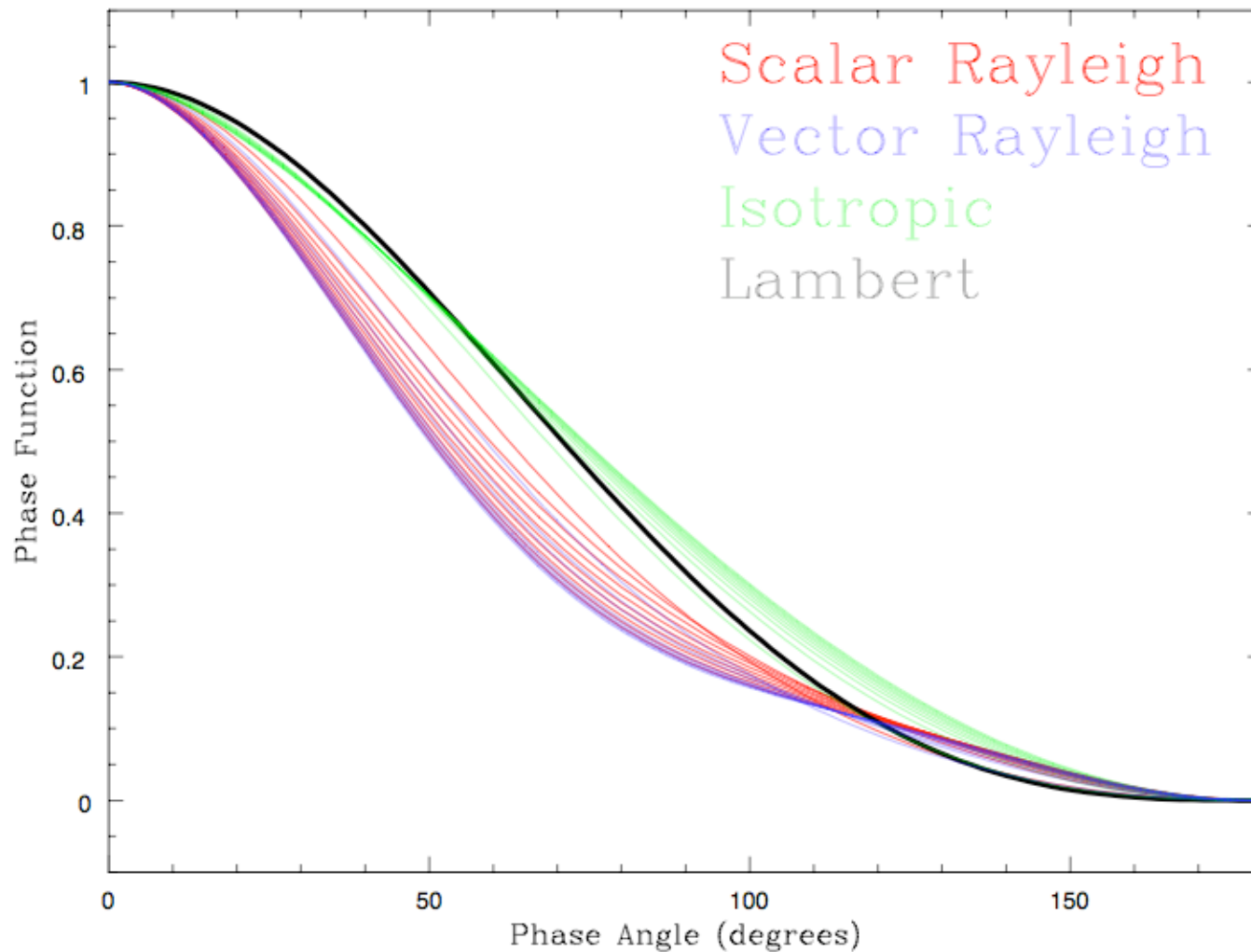
The optical light curve of an EGP with $a=1.5 \text{ AU}$ and $e=0.3$, assuming a G2V central star (a system similar to HD 160691; Jones et al. 2002) and an inclination of 80 degrees (with no transit effects). Three different possible viewing angles are shown (solid curves). Clouds condense and sublimate throughout each orbit as the planet-star distance varies in time. Shown for the sake of comparison are the light curves that would result if the object were to remain artificially cloud-free throughout its entire orbit (dashed curves).



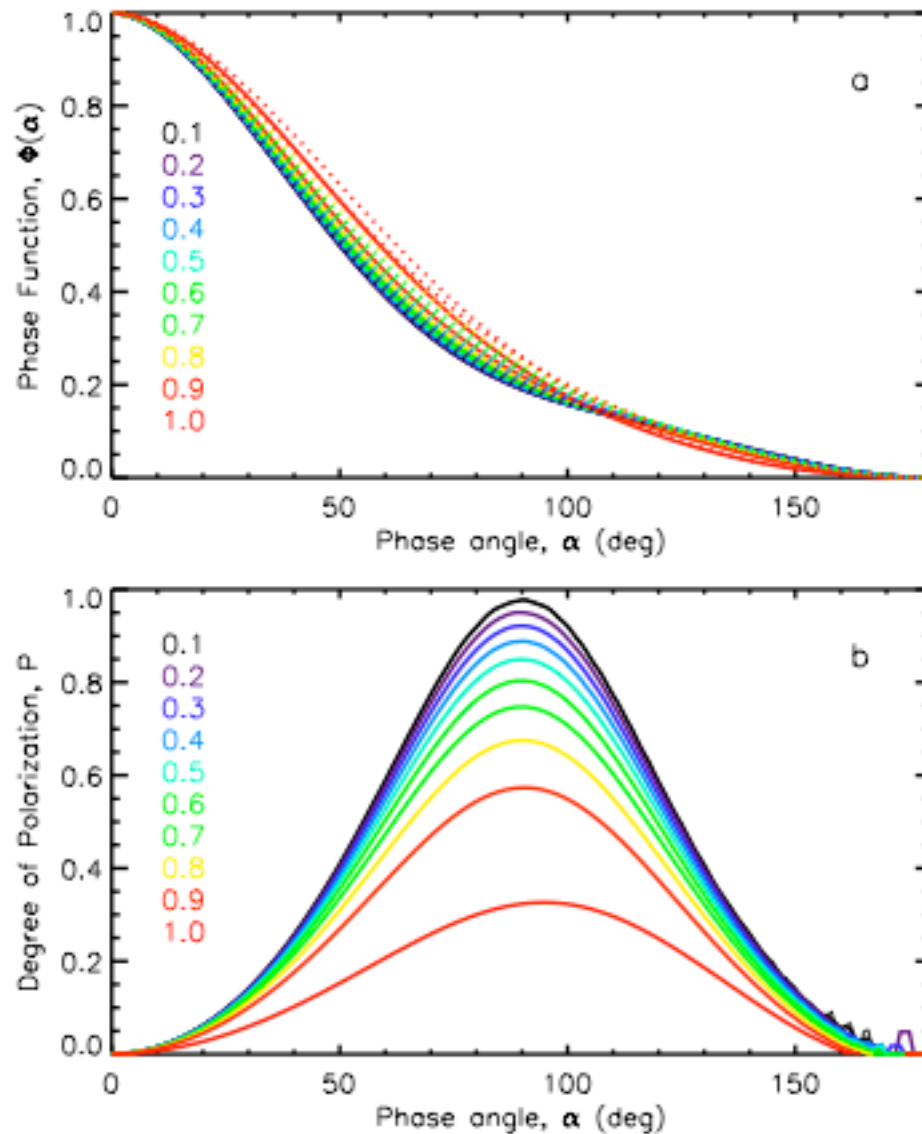
Coordinate system for calculating polarization due to reflection off planet.
(from Madhusudhan and Burrows 2011)



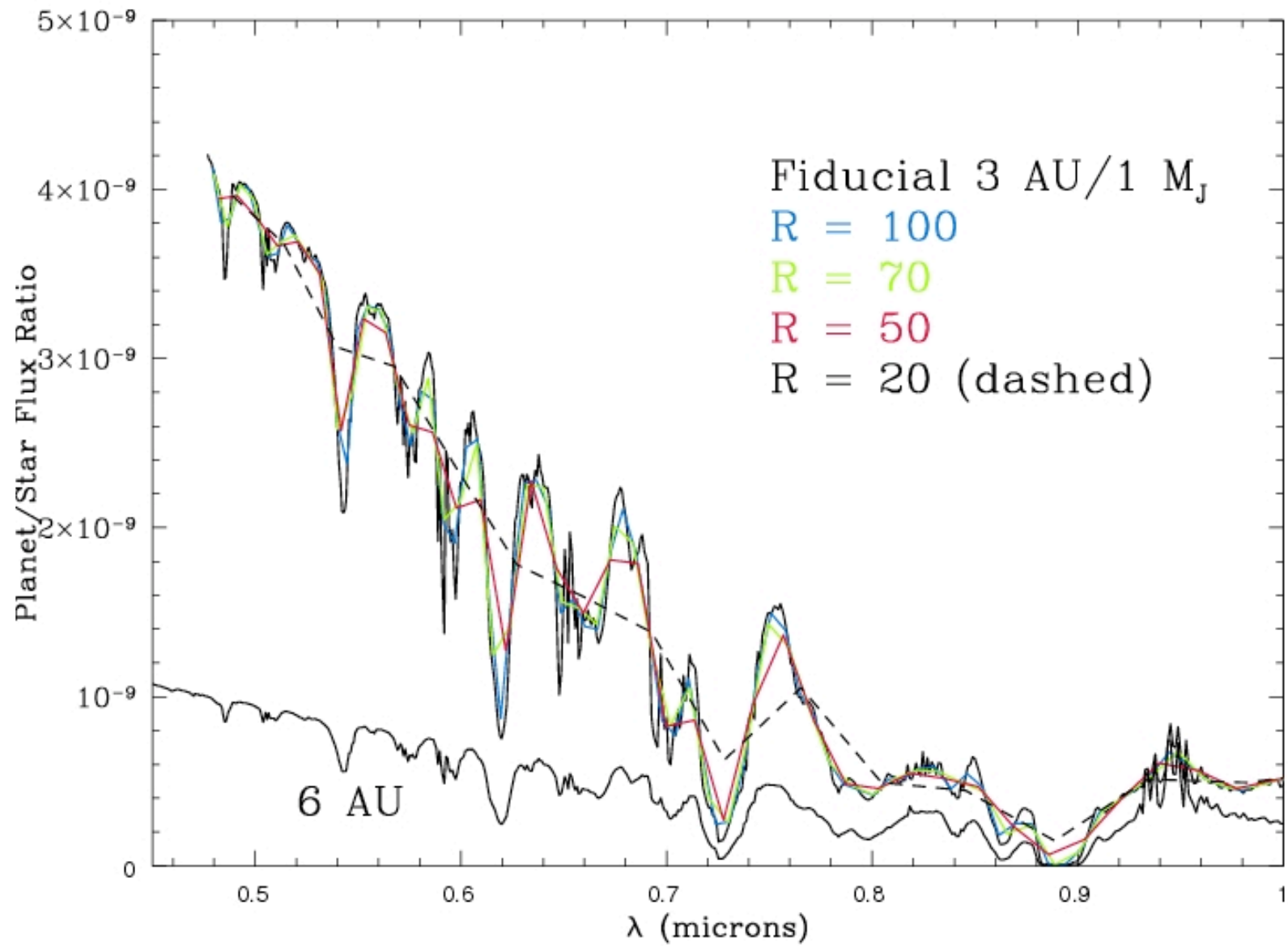
Comparison between phase curves due to Rayleigh scattering (with vector formulation) and Lambert scattering. The solid curves in the main panel show three phase curves for the cases described in the legend. The multi-colored dashed curves in the inset show the ratios between pairs of solid curves, e.g. the magenta-green dashed curve is the ratio between the magenta and green solid curves.



Comparison of phase curves for different scattering phase functions. The phase curves for Rayleigh scattering (both scalar and vector) and isotropic scattering are shown for several ω values between 0 and 1; higher phase curves correspond to larger ω . For Lambert scattering, the phase curve is independent of ω .



Phase curves and polarization for Rayleigh scattering. The different curves in each panel correspond to the different scattering albedos shown in the legend. In the upper panel, the solid curves show the phase curves for Rayleigh scattering using the vectorial Rayleigh phase matrix, whereas the dotted curves show those with the scalar phase function which does not incorporate polarization. The lower panel shows the degree of polarization (P), using the Rayleigh phase matrix. P is defined as $P = (Q^2 + U^2)^{1/2}/I$, where Q and U are the two Stokes parameters for linear polarization and I is the total intensity. For all the curves shown here, the orbit is assumed to be edge on ($i = 90$ degrees), in which case $U = 0$ and, hence, effectively $P = Q/I$.



References:

"Spectra and Diagnostics for the Direct Detection of Wide-Separation Extrasolar Giant Planets," (A. Burrows, D. Sudarsky, and I. Hubeny), *Astrophys. J.*, 609, 407, 2004.

"Theoretical Spectra and Atmospheres of Extrasolar Giant Planets" (D. Sudarsky, A. Burrows, and I. Hubeny), *Astrophys. J.*, 588, 1121, 2003.

"Phase Functions and Light Curves of Wide Separation Giant Planets," (David Sudarsky, Adam Burrows, Ivan Hubeny, and Aigen Li), *Astrophys. J.* 627, 520, 2005 (astro-ph/0501109).

"Albedo and Reflection Spectra of Extrasolar Giant Planets," (D. Sudarsky, A. Burrows, and P. Pinto) *Astrophys. J.*, 538, 885, 2000.

"The Theory of Brown Dwarfs and Extrasolar Giant Planets," (A. Burrows, W.B. Hubbard, J.I. Lunine, and J. Liebert), *Rev. Mod. Phys.*, 73, 719 (2001).

"Spectral and Photometric Diagnostics of Giant Planet Formation Scenarios," (D. Spiegel & A. Burrows), *Astrophys. J.*, 745, 174, 2012 (arXiv:1108.5172).

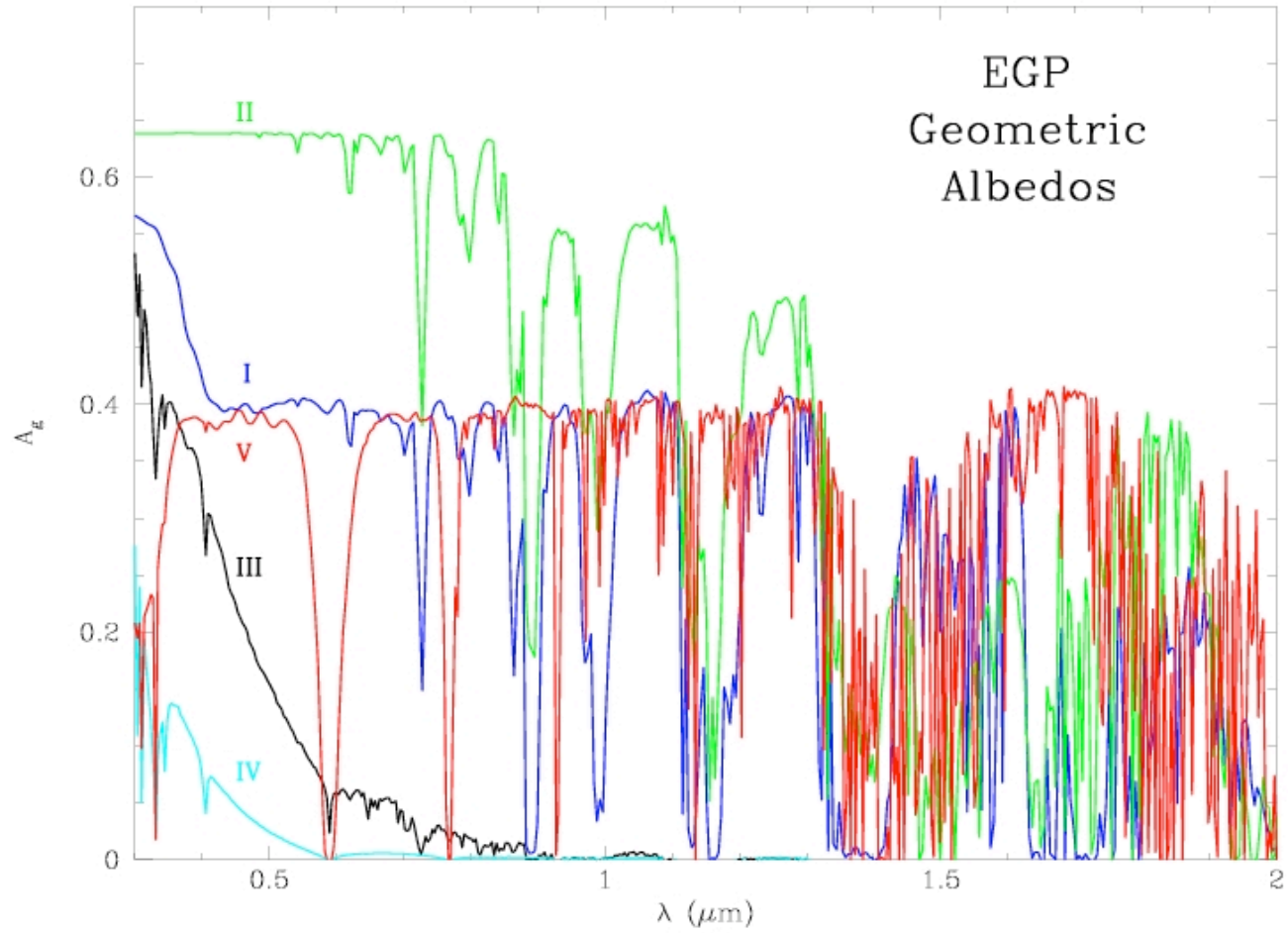
"Analytic Models for Albedos, Phase Curves, and Polarization of Reflected Light from Exoplanets," (N. Madhusudhan & A. Burrows), *Astrophys. J.*, 747, 25, 2011 (arXiv:1112.4476).

"A theoretical look at the direct detection of giant planets outside the Solar System," (A. Burrows) *Nature* 433, pp. 261 - 268, 2005 (astro-ph/0501484).

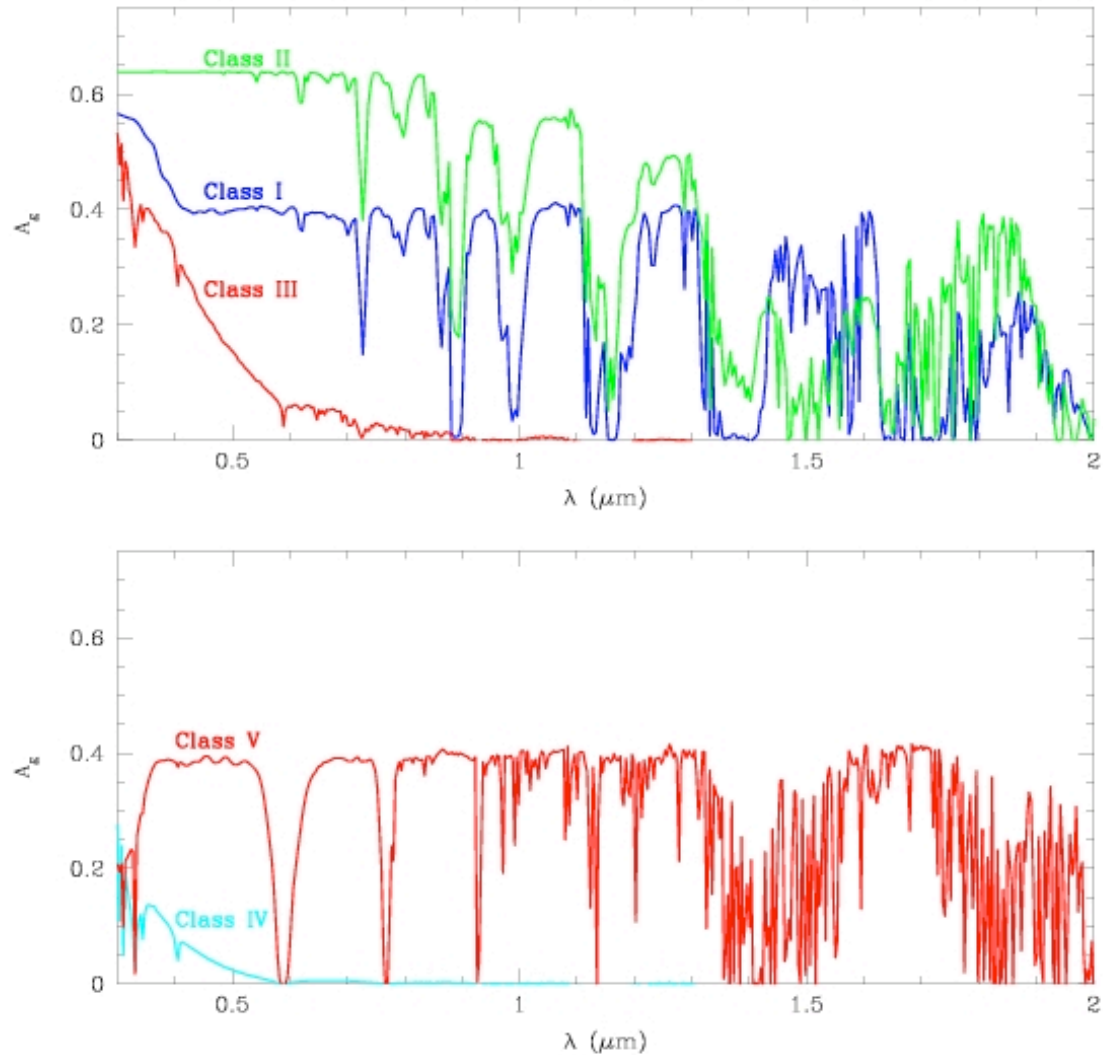
Extra Slides

Table 1. Interesting EGPs Listed by Angular Separation

EGP	separation ($''$)	star	a (AU)	d (pc)	P	Msini (M_J)	e
ϵ Eri b	1.0	K2V	3.3	3.2	6.85 yrs.	0.86	0.61
55 Cnc d	0.44	G8V	5.9	13.4	14.7	4.05	0.16
47 UMa c	0.28	G0V	3.73	13.3	7.10	0.76	0.1
Gl 777A b	0.23	G6V	3.65	15.9	7.15	1.15	~ 0
ν And d	0.19	F8V	2.50	13.5	3.47	4.61	0.41
HD 39091b	0.16	G1IV	3.34	20.6	5.70	10.3	0.62
47 UMa b	0.16	G0V	2.09	13.3	2.98	2.54	0.06
γ Cephei b	0.15	K2V	1.8	11.8	2.5	1.25	~ 0
HD 160691c	0.15	G3IV-V	2.3	15.3	3.56	~ 1	~ 0.8
14 Her b	0.15	K0V	2.5	17	4.51	3.3	0.33
HD 33636b	0.12	G0V	3.56	28.7	4.43	7.71	0.41
HD 10647b	0.12	F9V	2.10	17.3	2.89	1.17	0.32
HD 70642b	0.11	G5IV-V	3.3	29	4.79	2.0	0.10
HD 216437b	0.10	G4V	2.7	26.5	3.54	2.1	0.34
HD 147513b	0.098	G3V	1.26	12.9	1.48	1.0	0.52
HD 160691b	0.097	G3IV-V	1.48	15.3	1.74	1.7	0.31
HD 168443c	0.087	G5V	2.87	33	4.76	17.1	0.23
HD 50554b	0.077	F8V	2.38	31.03	3.50	4.9	0.42
HD 106252b	0.070	G0V	2.61	37.44	4.11	6.81	0.54
HD 10697b	0.067	G5IV	2.0	30	2.99	6.59	0.12
ν And c	0.061	F8V	0.83	13.5	241 days	2.11	0.18
GJ 876b	0.045	M4V	0.21	4.72	61.0	1.89	0.1
GJ 876c	0.028	M4V	0.13	4.72	30.1	0.56	0.27
HD 114762b	0.013	F9V	0.35	28	84.0	11.0	0.34
55 Cnc b	8.2×10^{-3}	G8V	0.12	13.4	14.7	0.84	0.02
ν And b	4.4×10^{-3}	F8V	0.059	13.5	4.62	0.71	0.034
51 Peg b	3.4×10^{-3}	G2V	0.05	14.7	4.23	0.44	0.01
τ Boo b	3.3×10^{-3}	F7V	0.05	15	3.31	4.09	~ 0
HD 209458b	9.6×10^{-4}	G0V	0.045	47	3.52	0.69	~ 0
HD 83443b	8.7×10^{-4}	K0V	0.038	43.5	2.99	0.35	0.08



Estimated geometric albedos of Class I through V EGPs.



(a) Estimated geometric albedos of Class I, II and III EGPs. A modified T-P profile model is used in each case. These conversions from spherical albedos are made by approximating the phase integral based on the single scattering albedo and scattering asymmetry factor at an atmospheric depth equal to the mean free path of incident radiation. (b) Estimated geometric albedos of Class IV and V EGPs.